Tumor necrosis factor is a necroptosis-associated alarmin

Francesca Pinci†, Moritz M. Gaidt†, Christophe Jung, Dennis Nagl, Gunnar Kuut and Veit Hornung*

Gene Center and Department of Biochemistry, Ludwig-Maximilians-Universität München, Munich, Germany

Necroptosis is a form of regulated cell death that can occur downstream of several immune pathways. While previous studies have shown that dysregulated necroptosis can lead to strong inflammatory responses, little is known about the identity of the endogenous molecules that trigger these responses. Using a reductionist *in vitro* model, we found that soluble TNF is strongly released in the context of necroptosis. On the one hand, necroptosis promotes TNF translation by inhibiting negative regulatory mechanisms acting at the post-transcriptional level. On the other hand, necroptosis markedly enhances TNF release by activating ADAM proteases. In studying TNF release at single-cell resolution, we found that TNF release triggered by necroptosis is activated in a switch-like manner that exceeds steady-state TNF processing in magnitude and speed. Although this shedding response precedes massive membrane damage, it is closely associated with lytic cell death. Further, we found that lytic cell death induction using a pore-forming toxin also triggers TNF shedding, indicating that the activation of ADAM proteases is not strictly related to the necroptotic pathway but likely associated with biophysical changes of the cell membrane upon lytic cell death. These results demonstrate that lytic cell death, particularly necroptosis, is a critical trigger for TNF release and thus qualify TNF as a necroptosis-associated alarmin.

KEYWORDS

TNF, alarmin, necroptosis, cell death, ADAM17

Introduction

Necroptosis is a lytic form of programmed cell death that can be triggered downstream of various immune receptors. Originally described to occur downstream of death receptors, necroptosis can be considered a "last resort type of response" of the cell, in that it is only engaged if other response pathways fail to be activated. This paradigm is well established in the context of TNF receptor 1 (TNFR1) signaling (1). Briefly, downstream of TNFR1 activation, Receptor-interacting serine/threonine-protein kinase 1 (RIPK1) can gain autophosphorylation activity when not ubiquitylated. Under

certain circumstances this results in the recruitment of RIPK3 *via* homotypic RHIM domain interaction. RIPK3 then forms homo-oligomers, in which RIPK3 is phosphorylated, which in turn leads to the recruitment and phosphorylation of mixed lineage kinase domain-like pseudokinase (MLKL) (2–5). Upon phosphorylation, MLKL oligomerizes and translocates to the plasma membrane, where it mediates membrane permeabilization and rupture by a so far not fully understood mechanism (6). Besides RIPK1-dependent pathways, two additional RHIM domain-containing molecules can also trigger RIPK3 activation and thus necroptosis. Downstream of Toll-like receptors 3 and 4 (TLR3 and TLR4), RIPK3 can be activated by the adapter protein TRIF (7, 8). In addition, the cytosolic sensor Z-DNA-binding protein 1 (ZBP1) can also recruit and activate RIPK3 (9, 10). As for RIPK1, the engagement of RIPK3 is dependent on RHIM domain-mediated homotypic interactions (11, 12). A well-known break on necroptosis induction is the catalytic activity of caspase-8 (1, 10, 13). In fact, caspase-8 plays an important role in cleaving and thus inhibiting RIPK1 and RIPK3 (14, 15).

Being involved downstream of immune receptors, it is believed that necroptosis has evolved as a host defense mechanism against pathogens (16). In line with this notion, necroptosis is utilized as a "backup" cell death pathway when apoptosis is blocked, for example by viral-encoded inhibitors (2, 16). Moreover, virus-encoded inhibitors of the RHIM domain as well as decoy viral MLKL (vMLKL) that counteract the activity of key necroptotic mediators exist, alluding to an important role of necroptosis in the control of infections (17–19).

Despite its beneficial contribution to pathogen clearance, necroptosis has also been reported to have a detrimental role in various inflammatory conditions that are not triggered by pathogens (20, 21). Evidence of a contribution of necroptosis to inflammatory diseases comprise abnormal expression of RIPK3, RIPK1 and MLKL observed in samples from Crohn´s Disease patients, suggesting a role of necroptosis in epithelial cell death and inflammation of the terminal ileum (22). In addition, homozygous mutations in the CASP8 gene leading to caspase-8 deficiency and increased necroptosis have been described in patients with very early onset inflammatory bowel disease (VEO-IBD) (23). Moreover, necroptosis has been implicated in the development of neurodegenerative and cardiovascular diseases, as well as in different liver disorders (20, 24). However, the complexity of these pathologies makes it difficult to establish necroptosis as a direct driver of inflammation. *In vivo* studies in *Ripk3* or *Mlkl*-deficient mice have been conducted to explore the role of necroptosis in different disease models. Nevertheless, discordant conclusions have been reported regarding the importance of necroptosis as an inducer of inflammation (20, 25).

The ability of necroptosis to promote inflammation is generally attributed to its lytic nature, which implies the release of its cellular content upon plasma membrane rupture.

Intracellular molecules may act as danger-associated molecular patterns (DAMPs) or alarmins upon release in the extracellular space. DAMPs are host-derived molecules that engage pattern recognition receptors (PRRs) in the context of cell damage or stress. This can be due to the release of molecules from certain circumscribed compartments into compartments that are normally devoid of these molecules (e.g. release of mitochondrial DNA into the cytoplasm) or the modification of endogenous molecules that render them PRR-agonistic (e.g. oxidization of lipids). Conceptually, DAMP-dependent PRR activation is a trade-off of the sensitivity of the PRR system and not intentional. Alarmins, on the other hand, are pre-formed molecules that are meant to engage pro-inflammatory signaling cascades upon extensive cell or tissue damage. This, for example, includes certain cytokines of the IL-1 family that are sequestered in the nucleus, lacking a secretion signal (e.g. IL-1α or IL-33) (26). These molecules are only released upon lytic cell death, engaging their dedicated cytokine receptors.

Despite the number of studies on necroptosis-mediated inflammation, the identity of molecules that may act as DAMPs or alarmins upon release by necroptotic cells remains elusive. Multiple reasons account for the difficulties in establishing a causative link between putative danger signals and necroptosis-mediated inflammation, including the use of immune stimuli to induce necroptosis, the necroptosis-independent inflammatory roles of RIPK3 (27) and the complexity of the investigated *in vivo* models (20). In light of these complications, we here sought to establish an *in vitro* system to explore the identity of necroptosis-associated DAMPs/alarmins that may be implicated in necroptosis-driven inflammation.

Results

A genetic system to study necroptosis-dependent inflammatory signaling

To study how necroptosis results in the release of pro-inflammatory mediators *in vitro*, we turned to BLaER1 monocytes as a model system. In the absence of caspase-8, these cells display a strong necroptotic phenotype following TLR4 stimulation (13). To this end, we employed $CASP8^{-/-}$ cells as necroptosis-prone cells and $CASP8^{-/-}$ x $MLKL^{-/-}$ cells as necroptosis resistant controls in a $CASP4^{-/-}$ genetic background, to prevent possible non-canonical inflammasome activation upon LPS stimulation (Figure S1A). As a proxy for lytic cell death, we measured LDH release, normalizing the values of a given treatment to an untreated control (0%) and a lysis control (100%). This normalization explains that for some conditions LDH release values below 0% were obtained. $CASP8^{-/-}$ cells, but not $CASP8^{-/-}$ x $MLKL^{-/-}$ cells, displayed robust necroptosis as evidenced by measuring LDH release in the supernatant (Figures 1A, S1B) or when assessing the
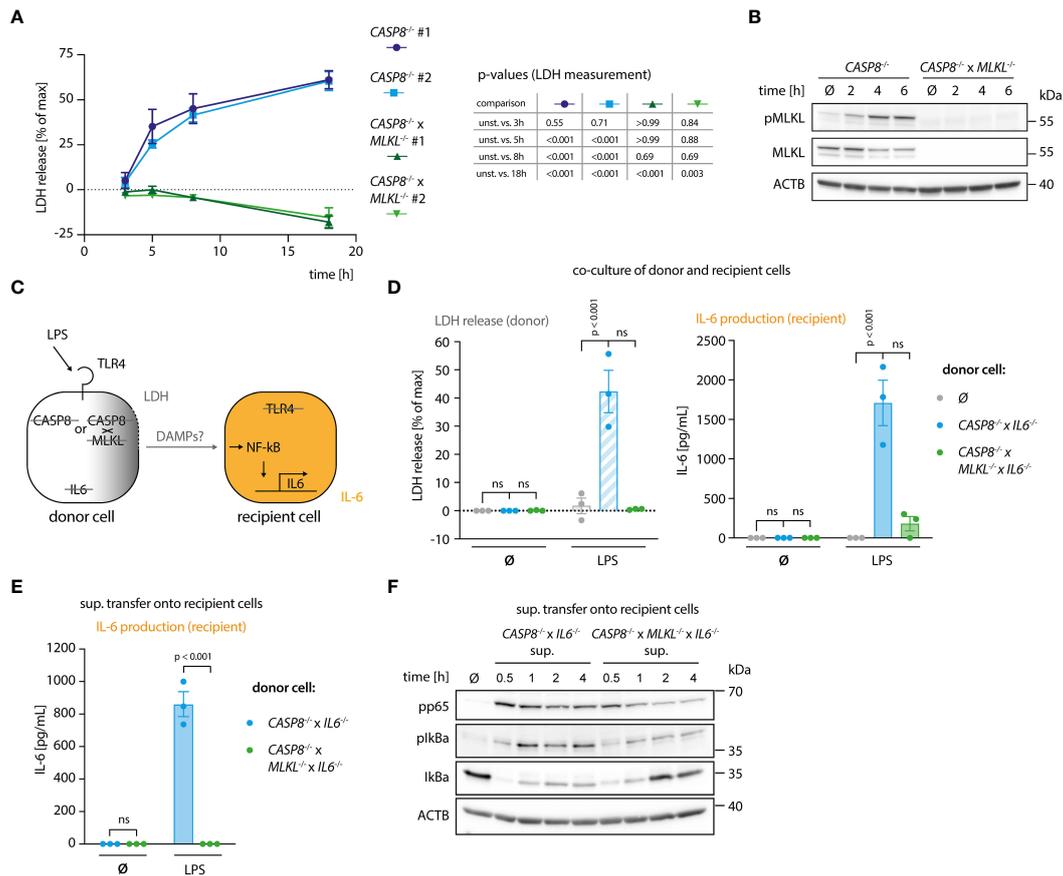
FIGURE 1

A genetic system to study necroptosis-dependent inflammation. **(A)** BLaER1 cells of the indicated genotypes were stimulated with 2 ng/ml LPS as indicated and LDH release was determined. **(B)** $CASP8^{-/-}$ and $CASP8^{-/-}$ x $MLKL^{-/-}$ BLaER1 macrophages were stimulated with 2 ng/ml LPS for the indicated times. Cell lysates were blotted for the indicated proteins. **(C)** Schematic overview of the system of donor and recipient BLaER1 cells generated to perform co-culture and supernatant transfer experiments. **(D)** Cells of the indicated genotypes were co-cultured in a 1:1 ratio with $TLR4^{-/-}$ recipient cells (grey dots = recipient cells only) and stimulated with 2 ng/ml LPS for 18 h LDH release and IL-6 production were determined. **(E)** Donor cells were stimulated with 2 ng/ml of LPS for 18 h The supernatant was then collected and used to stimulate $TLR4^{-/-}$ recipient cells for 24 h and IL-6 secretion was determined. **(F)** $CASP8^{-/-}$ x $IL6^{-/-}$ and $CASP8^{-/-}$ x $MLKL^{-/-}$ x $IL6^{-/-}$ cells were stimulated with 2 ng/ml LPS for 18 h and the supernatant was transferred on $TLR4^{-/-}$ recipient cells for the indicated period of times. Immunoblotting of the indicated proteins was performed on the lysates of stimulated $TLR4^{-/-}$ cells. Data are depicted as mean $\pm$ SEM of 3 independent experiments **(A, D, E)** or as one representative experiment of two independent experiments **(B, F)**. Statistics indicate significance by a repeated measures two-way ANOVA **(A)** or a two-way ANOVA **(D, E)** with either a Dunnett **(A, D)** or Šidák **(E)** correction for multiple testing. P values as indicated or ns, not significant.

phosphorylation status of MLKL (Figure 1B). To address whether necroptotic cells can trigger inflammatory responses in bystander cells, we devised a system in which we could co-culture cells undergoing necroptosis (donor cells) with cells that were insensitive to necroptosis induction (recipient cells). In this setting, we measured interleukin-6 (IL-6) production in recipient cells as a proxy for pro-inflammatory gene expression (Figure 1C). IL-6 was chosen for its high sensitivity and dynamic range as an NF-κB target gene. The *IL6* gene was deleted in the donor cell population, so that all IL-6 measured in this setup can be ascribed to recipient cells. Apart from its intended phenotype, IL-6 deficiency had no impact on necroptosis or pro-inflammatory gene expression in donor

cells (Figures S1C–E). Further, since LPS is used in this model to trigger necroptosis in donor cells, we rendered recipient cells insensitive to LPS by disrupting the *TLR4* gene (Figure 1C). Donor and recipient cells were then co-cultured and analyzed for LDH release, as well as IL-6 production. As expected, co-cultures containing $CASP8^{-/-}$ donor cells that were additionally deficient for IL-6 displayed a marked release of LDH into the supernatant upon LPS treatment (Figure 1D, left panel). This response was not seen when $CASP8^{-/-}$ x $MLKL^{-/-}$ donor cells were used. Intriguingly, when co-cultured with necroptosing donor cells but not $CASP8^{-/-}$ x $MLKL^{-/-}$ cells, a strong IL-6 response was seen in recipient cells (Figure 1D, right panel). To explore whether this pro-inflammatory activity of necroptosis required cell-to-

cell contact, we next conducted experiments, in which we transferred supernatant from necroptosing donor cells or control conditions onto recipient cells. Analogous to the co-culture conditions, a potent IL-6 response was seen when supernatant from stimulated $CASP8^{-/-}$ cells was transferred (Figure 1E). In line with these results, transfer of supernatant from necroptosing donor cells led to NF-κB activation in recipient cells as evidenced by p65 and IκBα phosphorylation, as well as IκBα degradation (Figure 1F). Altogether, these results indicated that necroptosis-driven inflammatory responses can be recapitulated in an *in vitro* system, and that cell-to-cell contact is not required to evoke pro-inflammatory activity.

Necroptosis-driven inflammatory responses are mediated by TNF

Our results indicated that the necroptosis-driven inflammatory response in bystander cells is largely mediated by a soluble factor. Further, considering the experimental setup that made use of $TRL4^{-/-}$ recipient cells, we could exclude a TLR4-agonistic molecule as the mediator of this response. Prolonged incubation at 75°C resulted in a complete loss of the pro-inflammatory activity of the necroptotic supernatant, indicating that a proteinaceous component might play a critical role in its activity (Figure S2A). Since triggering necroptosis in myeloid cells leads to secondary NLRP3 inflammasome activation (28, 29), we asked whether IL-1β would be responsible for IL-6 secretion in recipient cells. To address this, we induced necroptosis in donor cells in the absence or presence of the NLRP3 inhibitor MCC950 (30). As expected, necroptotic cells secreted IL-1β, which was readily blocked by MCC950 (Figure S2B). However, blocking IL-1β secretion did not impact on IL-6 secretion by $TRL4^{-/-}$ recipient cells, excluding a role of IL-1β as an alarmin in our model system (Figure S2C). To further explore the possibility that a proteinaceous component might mediate the pro-inflammatory response in recipient cells, we separated the supernatant of necroptotic cells using size exclusion chromatography (SEC). To obtain a large volume of necroptotic supernatant, we switched to THP-1 cells as donor cells. We engineered these cells to undergo necroptosis upon expression of a dominant active MLKL construct ($MLKL^{1-201}$) that is sufficient to induce cell death (Figure S2D) (31). Such engineered cells underwent necroptosis as expected and upon transfer, the supernatant of these cells triggered IL-6 production in recipient cells (Figures S2D, E). We then subjected supernatant of control or necroptosing THP-1 cells to SEC and tested the individual fractions for pro-inflammatory activity on recipient cells (Figures 2A–E). These experiments revealed that the IL-6 inducing activity eluted at around 15 - 17 ml of the column volume, which corresponds to proteins of approximately 20-70 kDa in size. As a complementary approach, we also generated recipient cells, in which we deleted essential

signaling hubs for various PRR systems. To block TLRs and cytokines of the IL-1 family, we deleted *MYD88* and *TICAM1* (TRIF), to prevent RLR and cGAS-dependent activation, we deleted *MAVS* and *STING1* (STING), and to block TNF and Lymphotoxin-α (LTA)-dependent pro-inflammatory gene expression we deleted *TNFRSF1A* (TNFR1) (Figures 2F, S2F). Transferring necroptotic supernatant onto these cells in the presence of the TLR4 inhibitor CLI095 to inhibit LPS-driven effects, revealed that $TNFRSF1A^{-/-}$ cells showed a markedly decreased IL-6 response, whereas the perturbation of the other signaling hubs had no impact (Figure 2G). MyD88/TRIF and MAVS/STING deficient cells used in this assay were produced in a wildtype (WT) background, while TLR4 and TNFR1 deficient cells were generated from caspase-4-deficient cells. As such, we additionally conducted the supernatant transfer experiment to compare WT and $CASP4^{-/-}$ cells in their response to the necroptotic supernatant. Caspase-4 deficiency did not account for a different behavior of these recipient cells in our supernatant transfer assay (Figure S2G). To elucidate whether this TNFR1-dependent activity required either TNF, LTA, or both, we generated donor cells, in which these cytokines were deleted (Figure 2H). None of these perturbations impacted on necroptosis induction (Figure 2H, left panel). However, TNF-deficient donor cells failed to trigger IL-6 production in recipient cells, whereas LTA deficiency had no impact (Figure 2H, middle and right panel). Since these results pointed to TNF as the main driver of pro-inflammatory gene expression in bystander cells, we next assessed TNF production of the donor cell population as a function of necroptosis induction. These experiments revealed that TNF secretion was markedly increased in cells that underwent necroptosis, with peak levels being reached already 4 hours after stimulation (Figure 2I). Importantly, TNF release by LPS-stimulated $CASP8^{-/-}$ cells could be reduced by treatment with the RIPK3 inhibitor GSK'872, ruling out that clonal differences may account for the divergence in TNF secretion between $CASP8^{-/-}$ and $CASP8^{-/-}$ x $MLKL^{-/-}$ cells (Figure S2H). In summary, these results indicated that necroptosis-driven induction of pro-inflammatory gene expression is largely driven by TNF in this model. Moreover, these data suggested that necroptosis strongly enhanced TNF secretion.

Necroptosis boosts TNF translation and enhances TNF shedding

As a key pro-inflammatory mediator, TNF is controlled at multiple levels. Next to being regulated at the level of transcription, the translation of TNF mRNA is heavily controlled at the post-transcriptional level. To this end, several cis-elements within the 3' UTR of TNF have been identified that are regulated by various trans-activating factors that repress TNF mRNA translation or induce decay of its mRNA (32–36). Moreover, the availability of the protein itself in the extracellular *milieu* is also regulated. As such,
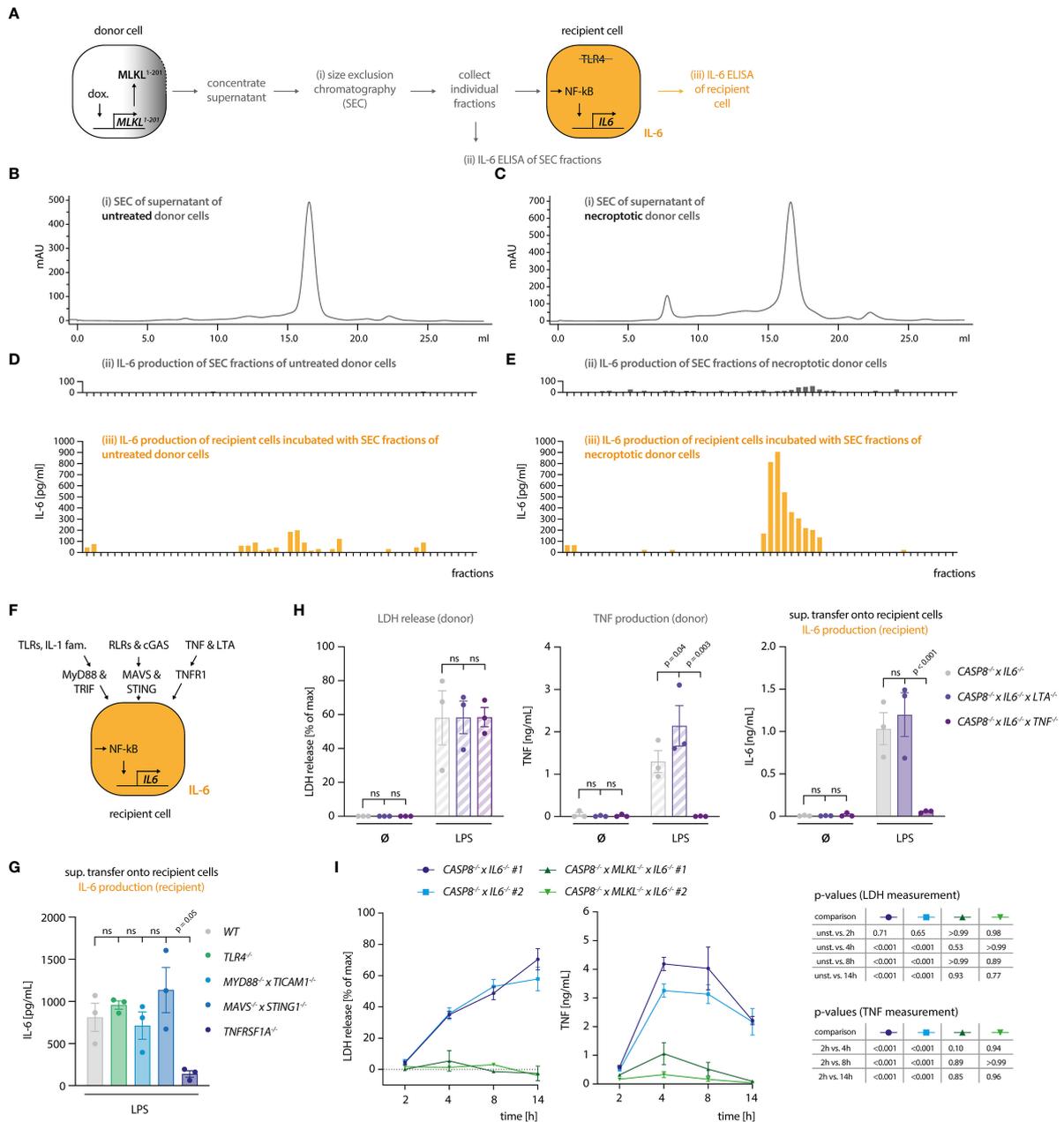
FIGURE 2

Necroptosis-driven inflammatory responses are mediated by TNF. **(A)** Schematic overview of the SEC experiment. **(B, C)** Chromatograms of the SEC of the supernatant of THP1 MLKL$^{1-201}$ cells left untreated **(B)** or stimulated with 1 µg/ml doxycycline for 16 h **(C)**. **(D, E)** IL-6 measurement in SEC fractions of untreated and treated THP1 MLKL$^{1-201}$ cells (in grey, upper graphs) and IL-6 production of TLR4$^{-/-}$ BLaER1 recipient cells after incubation with SEC fractions for 14 h (in orange, lower graphs). **(F)** Scheme of knock-out generation in BLaER1 recipient cells to invalidate specified innate immune pathways. BLaER1 cells deficient for the indicated pathways were subsequently tested in the supernatant transfer assay. **(G)** Recipient cells of the indicated genotypes were incubated for 24 h with the supernatant of CASP8$^{-/-}$ x IL6$^{-/-}$ donor cells stimulated for 18 h with 2 ng/ml LPS. To block LPS-dependent effects, the TLR4 inhibitor CLI095 was added to recipient cells at the concentration of 1 µg/ml. IL-6 production of recipient cells was measured. **(H)** BLaER1 cells of the indicated genotypes were stimulated with 2 ng/ml LPS or left untreated for 18 h, after which LDH and TNF release were measured. The supernatant of these cells was utilized to stimulate TLR4$^{-/-}$ BLaER1 cells. IL-6 release by TLR4$^{-/-}$ cells was measured 24 h thereafter. **(I)** BLaER1 cells of the indicated genotypes were stimulated with 2 ng/ml LPS for the indicated time points. LDH release and TNF secretion from donor cells of the specified genotypes were measured at the indicated time points. Data are depicted as mean ± SEM of 3 independent experiments **(G–I)** or as one representative experiment of two independent experiments **(B-E)**. Statistics indicate significance by one-way **(G)** or two-way ANOVA **(H)** or a repeated measures two-way ANOVA **(I)** with a Dunnett **(G–I)** correction for multiple testing. P values as indicated or ns, not significant.

being produced as a type II transmembrane protein, TNF needs to be cleaved by membrane metalloproteases to be released. This step is mainly regulated by ADAM17 and to a lesser extent by ADAM10 (37–40). Comparing $CASP8^{-/-}$ cells with $CASP8^{-/-}$ x $MLKL^{-/-}$ revealed no significant difference in TNF mRNA expression between these two cell types (Figure 3A), thereby excluding the possibility of enhanced TNF mRNA transcription. However, when we measured TNF protein expression, we observed both higher amounts of pro-TNF levels in cell lysates as well as increased levels

of cleaved TNF in the supernatant, suggesting that regulation of TNF expression and shedding may both contribute to enhanced TNF release (Figure 3B). Of note, $CASP8^{-/-}$ and $CASP8^{-/-}$ x $MLKL^{-/-}$ cells produced similar amounts of IL-6 and IL-8, showing that other pro-inflammatory cytokines transactivated by NF-κB were not affected by these genotypes. As such, both IL-6, as well as IL-8 levels did not show any differences between $CASP8^{-/-}$ and $CASP8^{-/-}$ x $MLKL^{-/-}$ cells (Figures S1C, D). Speculating that necroptosis impacted on the post-transcriptional regulation of TNF mRNA
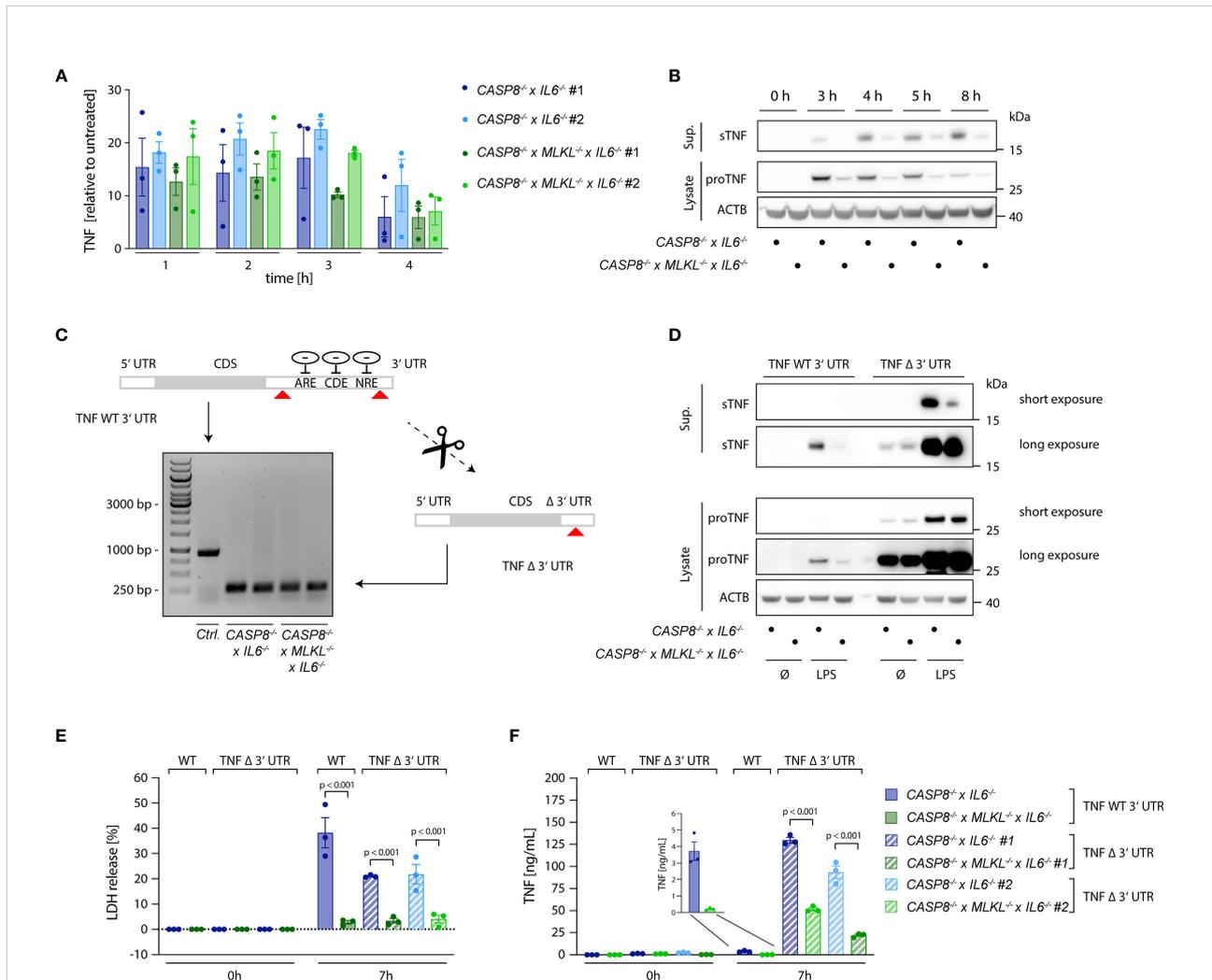
FIGURE 3

Necroptosis boosts TNF translation. **(A)** qPCR of TNF induced upon stimulation with 2 ng/ml LPS in the indicated cells. Results are shown as fold change relative to unstimulated cells. **(B)** Immunoblotting of pro-TNF (cell lysates) and sTNF (supernatants) of $CASP8^{-/-}$ x $IL6^{-/-}$ and $CASP8^{-/-}$ x $MLKL^{-/-}$ x $IL6^{-/-}$ cells upon stimulation with 2 ng/ml LPS for the indicated time points. ACTB was detected as loading control. **(C)** $CASP8^{-/-}$ and $CASP8^{-/-}$ x $MLKL^{-/-}$ BLaER1 cells deficient for the 3'UTR of the TNF gene (TNF Δ 3'UTR) were generated by employing two gRNAs targeting the 3'UTR at its very beginning and very end, respectively (red arrows). The removal of the 3'UTR was assessed by PCR (Control = long PCR product, TNF Δ 3'UTR = short PCR product). Two clones of TNF Δ 3'UTR are shown per parental genotype. **(D)** BLaER1 cells of the indicated genotypes were stimulated with LPS (2 ng/ml) for 7 h pro-TNF expression and matured TNF were assessed by immunoblotting. **(E, F)** BLaER1 cells of the indicated genotypes were stimulated with LPS (2 ng/ml) for 7 h. Cell death was evaluated by LDH assay **(E)**. Secreted TNF was measured by ELISA **(F)**. Data are depicted as mean ± SEM of three independent experiments or as one representative immunoblot of three independent experiments **(B, D)**. Statistics indicate significance by two-way ANOVA with a Tukey correction for multiple testing **(E, F)**, whereas p values are as indicated. Statistics for data in **(A)** were calculated using a repeated measures two-way ANOVA, whereas none of the comparisons reached statistical significance (not depicted).

translation *via* its 3' UTR, we generated *CASP8*^{-/-} and *CASP8*^{-/-} x *MLKL*^{-/-} cells, in which we deleted the 3′UTR of the TNF gene (TNF Δ 3′UTR) (Figure 3C). Doing so, we eliminated all critical cis-controlling elements that negatively affect the stability or translation of TNF mRNA, while we left the poly adenylation signal intact. As a result, pro-TNF expression levels were dramatically increased in both *CASP8*^{-/-} and *CASP8*^{-/-} x *MLKL*^{-/-} cells and considerable amounts of pro-TNF expression were already observed in lysates of unstimulated cells (Figure 3D). Importantly, removing the 3' UTR resulted in similar expression levels of pro-TNF for both necroptotic and non-necroptotic cells (Figure 3D), indicating that necroptosis indeed impacts on the negative regulation of TNF mRNA translation through its 3' UTR. In this setting, we could now investigate the impact of necroptosis on TNF shedding. Indeed, despite similar expression of pro-TNF, *CASP8*^{-/-} cells still exhibited 3-4x higher levels of soluble TNF in the supernatant upon necroptosis induction (Figures 3D-F). Altogether, these results suggested that increased secretion of mature TNF during necroptosis depends on higher pro-TNF expression, by alleviating negative regulatory pathways at the post-transcriptional level, as well as enhanced TNF shedding.

Necroptosis enhances TNF shedding

To explore how necroptosis impacts on TNF shedding, we used 293T cells as a heterologous expression system, in which we could dissociate TNF expression from shedding. To induce necroptosis, we expressed the autoactive MLKL[1-201] construct, while using an inactive MLKL variant (MLKL[1-154]) or mCherry as a control (31). Of note, this reductionist setting could also rule out RIPK3-dependent effects on necroptosis-dependent TNF secretion. MLKL[1-201]-dependent necroptosis induction led to a marked release of LDH from 293T cells, while the other conditions showed little activity (Figure 4A, left panel). Concomitant with cell death, a strong TNF signal in the supernatant was detected by ELISA (Figure 4A, right panel). This increase in TNF within the supernatant was due to a markedly enhanced pro-TNF conversion to soluble TNF, as evidenced by immunoblot. Importantly, the release of IL-6, which does not require shedding for its maturation, was not enhanced upon necroptosis induction in these settings (Figure S3A). To confirm that necroptosis indeed resulted in increased TNF shedding and not in a passive release of pro-TNF, we additionally conducted experiments in 293T cells lacking ADAM10 and ADAM17 (41). In these cells, TNF release upon necroptosis was severely impaired, while ADAM10/17 deficiency had no impact on cell death following MLKL[1-201] expression (Figure 4B). Analogous results were obtained when studying TNF levels in lysates or supernatant by immunoblot (Figure 4B, lower right panel). Next, we sought to investigate the role of ADAM proteases in the BLaER1 cell model. RNA-seq analysis revealed that ADAM10, ADAM17 and ADAM9 are the

main ADAM proteases expressed in these cells and that LPS positively modulates their expression (Figure S3B). With ADAM17 and ADAM10 being the main TNF sheddases described, we generated BLaER1 cells lacking either of these two enzymes (Figure S3C) to address their role in necroptosis-dependent TNF shedding. Doing so revealed that ADAM17 was the predominant enzyme required for TNF shedding in the context of necroptosis, while neither ADAM17 nor ADAM10 had a significant impact on cell death induction (Figure 4C, left and middle panel). Consistent with this notion, supernatant from *ADAM17*^{-/-} but not control or *ADAM10*^{-/-} cells displayed a markedly reduced activity in the bystander cell activation assay (Figure 4C, right panel). Additionally, the secretion of another known target of ADAM17, IL-6Rα (42), increased in necroptotic BLaER1 cells compared to control cells (Figure S3D). Altogether, these results indicated that necroptosis drives enhanced TNF-dependent inflammatory responses in two ways: on the one hand, necroptosis results in enhanced TNF translation, and on the other hand, necroptosis triggers TNF shedding in a predominantly ADAM17-dependent manner.

Necroptosis triggers shedding activity in a switch-like fashion

To explore the spatiotemporal relationship of necroptosis and TNF shedding, we made use of a TNF shedding reporter construct (C-tag TNF) that allows the monitoring of TNF maturation at the ADAM17 cleavage site in real time (41). Upon cleavage, this construct exposes a neo C-terminus that serves as an epitope for a nanobody that only binds the cleaved version of this reporter. This construct was additionally equipped with an N-terminal mCherry tag, to monitor the subcellular localization of TNF. Cells expressing the C-tag reporter displayed the same gain in TNF shedding upon necroptosis induction as cells expressing unmodified TNF (Figure S4A). Using a fluorescently labeled nanobody, we monitored the C-tag signal as a function of MLKL[1-201]-induced necroptosis in control cells, as well as in *ADAM10*^{-/-} x *ADAM17*^{-/-} deficient cells. In addition, we also measured C-tag positivity in controls not undergoing necroptosis. 4.5 hours following necroptosis induction, we observed a strong signal for the C-tag nanobody at the plasma membrane of cells that also showed signs of necroptosis (Figures 5A, B, and Supplementary Video S1). This signal was completely abrogated in cells lacking ADAM10/17, which still displayed membrane-associated expression of TNF (Figures 5A, B, and Supplementary Video S2). Control cells not undergoing necroptosis, also showed a C-tag reactive signal, yet with marked lower intensity (Figures 5A, B, and Supplementary Video S3). Time-lapse analysis revealed that cells undergoing necroptosis became positive for the C-tag signal within 30-40 minutes (Figures 5B, C). Quantifying the C-tag signal and
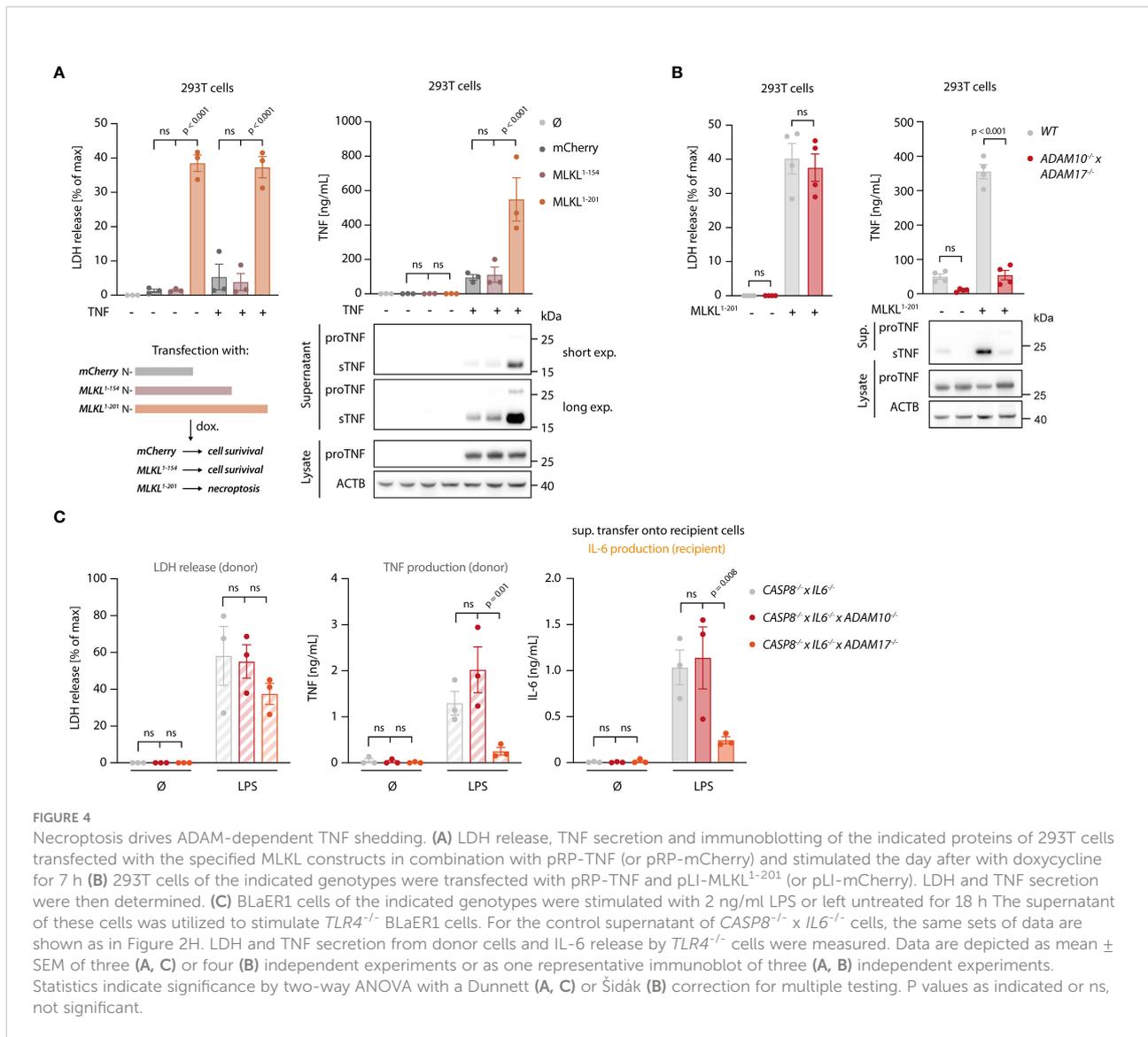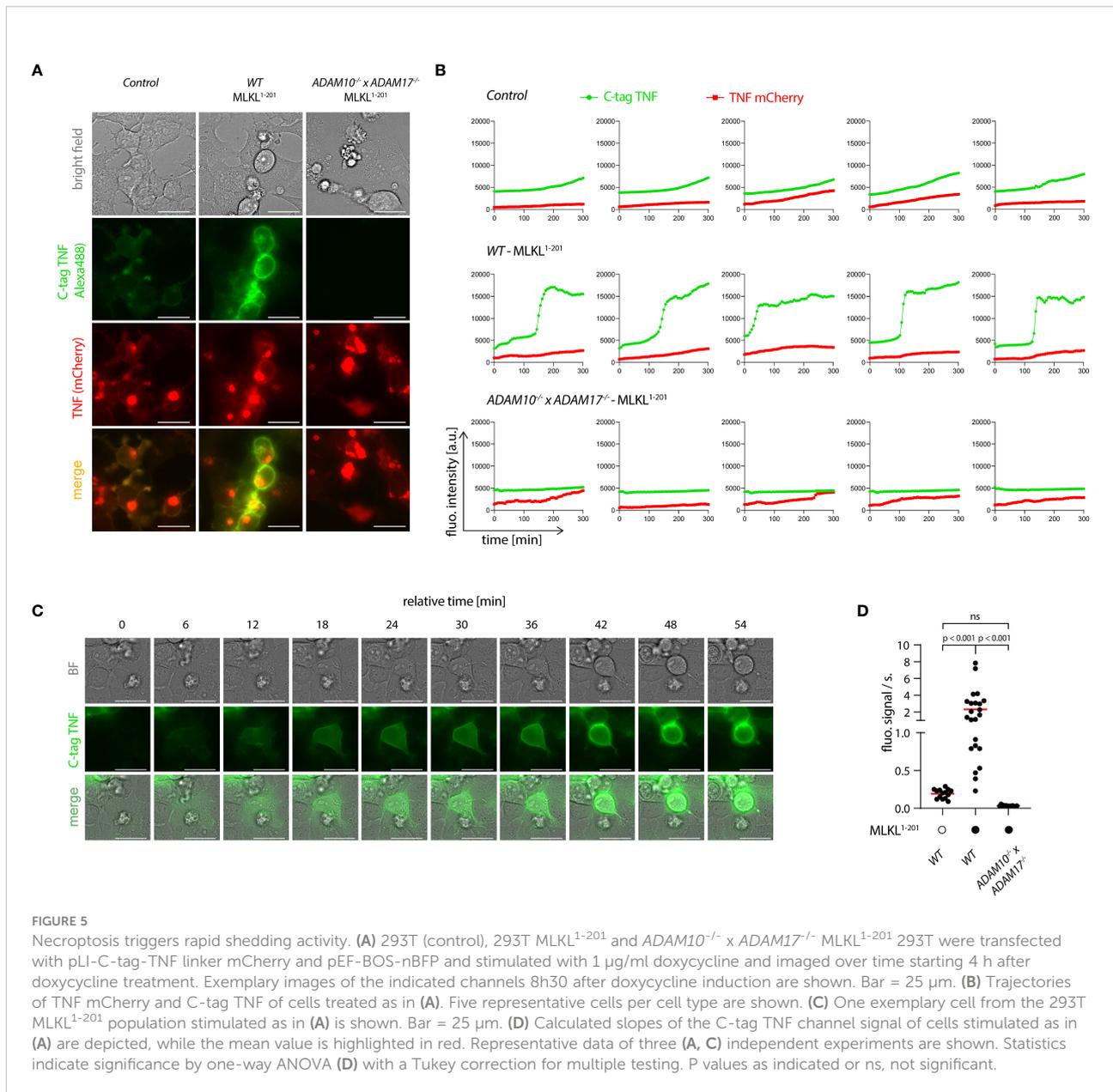
FIGURE 4

Necroptosis drives ADAM-dependent TNF shedding. **(A)** LDH release, TNF secretion and immunoblotting of the indicated proteins of 293T cells transfected with the specified MLKL constructs in combination with pRP-TNF (or pRP-mCherry) and stimulated the day after with doxycycline for 7 h **(B)** 293T cells of the indicated genotypes were transfected with pRP-TNF and pLI-MLKL$^{1-201}$ (or pLI-mCherry). LDH and TNF secretion were then determined. **(C)** BLaER1 cells of the indicated genotypes were stimulated with 2 ng/ml LPS or left untreated for 18 h The supernatant of these cells was utilized to stimulate $TLR4^{-/-}$ BLaER1 cells. For the control supernatant of $CASP8^{-/-}$ x $IL6^{-/-}$ cells, the same sets of data are shown as in Figure 2H. LDH and TNF secretion from donor cells and IL-6 release by $TLR4^{-/-}$ cells were measured. Data are depicted as mean ± SEM of three **(A, C)** or four **(B)** independent experiments or as one representative immunoblot of three **(A, B)** independent experiments. Statistics indicate significance by two-way ANOVA with a Dunnett **(A, C)** or Šidák **(B)** correction for multiple testing. P values as indicated or ns, not significant.

analyzing the slope for several cells individually revealed that cells undergoing necroptosis indeed displayed a rapid, switch-like gain in TNF shedding. On the other hand, the gain in C-tag signal for cells not undergoing necroptosis was only gradual, and it never reached the same level as necroptosing cells in the time frame studied (Figures 5B, D). Similar to apoptosis, necroptosis also results in the externalization of phosphatidylserine phospholipids to the outer leaflet of the membrane (43). Measuring Annexin V positivity next to TNF shedding, we observed that these two events were closely correlated, with the individual slopes of the gain in fluorescent signal being comparable (Figures S4B–D). However, C-tag positivity preceded Annexin V positivity by a mean value of 24 minutes (Figure S4E). Studying PI positivity as a proxy for membrane permeabilization, we observed that cells undergoing necroptosis

and TNF shedding displayed a delayed gain in PI signal (Figures S4F-I). In comparison to Annexin V, this delay was even more pronounced with a mean difference of 53 minutes (Figure S4I). Further, analyzing the slope of the gain in PI positivity revealed that this event occurred more rapidly than the TNF shedding event (Figures S4G, H). This was also reflected in the slope of the PI signal which was approximately twice the value of the C-tag signal (Figure S4H). Altogether, these results indicated that necroptosis-induced TNF shedding is a rapid event that differs from the steady state shedding process in magnitude and kinetics. As such, it displays a switch-like behavior, in which TNF shedding occurs in a time frame of 30-40 minutes. In the course of cell death, TNF shedding precedes the outward flipping of phosphatidylserine phospholipids, which is followed by membrane permeabilization.

FIGURE 5

Necroptosis triggers rapid shedding activity. **(A)** 293T (control), 293T MLKL[1-201] and *ADAM10*^{-/-} x *ADAM17*^{-/-} MLKL[1-201] 293T were transfected with pLI-C-tag-TNF linker mCherry and pEF-BOS-nBFP and stimulated with 1 µg/ml doxycycline and imaged over time starting 4 h after doxycycline treatment. Exemplary images of the indicated channels 8h30 after doxycycline induction are shown. Bar = 25 µm. **(B)** Trajectories of TNF mCherry and C-tag TNF of cells treated as in **(A)**. Five representative cells per cell type are shown. **(C)** One exemplary cell from the 293T MLKL[1-201] population stimulated as in **(A)** is shown. Bar = 25 µm. **(D)** Calculated slopes of the C-tag TNF channel signal of cells stimulated as in **(A)** are depicted, while the mean value is highlighted in red. Representative data of three **(A, C)** independent experiments are shown. Statistics indicate significance by one-way ANOVA **(D)** with a Tukey correction for multiple testing. P values as indicated or ns, not significant.

Enhanced TNF shedding is a general phenomenon of lytic cell death rather than a specific necroptosis-related feature.

Our data thus far indicated that necroptosis triggers both TNF translation and shedding and that the latter takes place in the early stages of cell death, before massive membrane damage. Live cell imaging experiments revealed that TNF shedding occurs as a switch-like phenomenon and appears to be strictly related to physical changes of the cell membrane before membrane permeabilization. We therefore asked whether the mechanism behind increased TNF shedding is specifically

related to the necroptotic pathway or if it is promoted by changes in membrane integrity during lytic cell death in general. To address this question, we applied a model in which we can induce lytic cell death by adding an exogenous pore-forming molecule, namely the pore-forming toxin streptolysin O (SLO) from *S. pyogenes* (44, 45). As for the MLKL gain-of-function studies, we used HEK 293T cells overexpressing pro-TNF that we then challenged with exogenous SLO. As expected, SLO treatment led to lytic cell death, as indicated by LDH release (Figure 6A, left panel). Similar to the overexpression of MLKL[1-201], SLO-mediated cell death was accompanied by massive TNF secretion due to enhanced shedding, as evidenced by ELISA and immunoblot (Figure 6A, right panel and Figure 6B).

Importantly, IL-6 secretion was not enhanced upon SLO-mediated cell death, but rather decreased due to cell death during the experiment (Figure 6C). In conclusion, these data indicate that enhanced TNF shedding is linked to the membrane dynamics upon lytic cell death rather than being a specific feature of the necroptotic pathway itself.

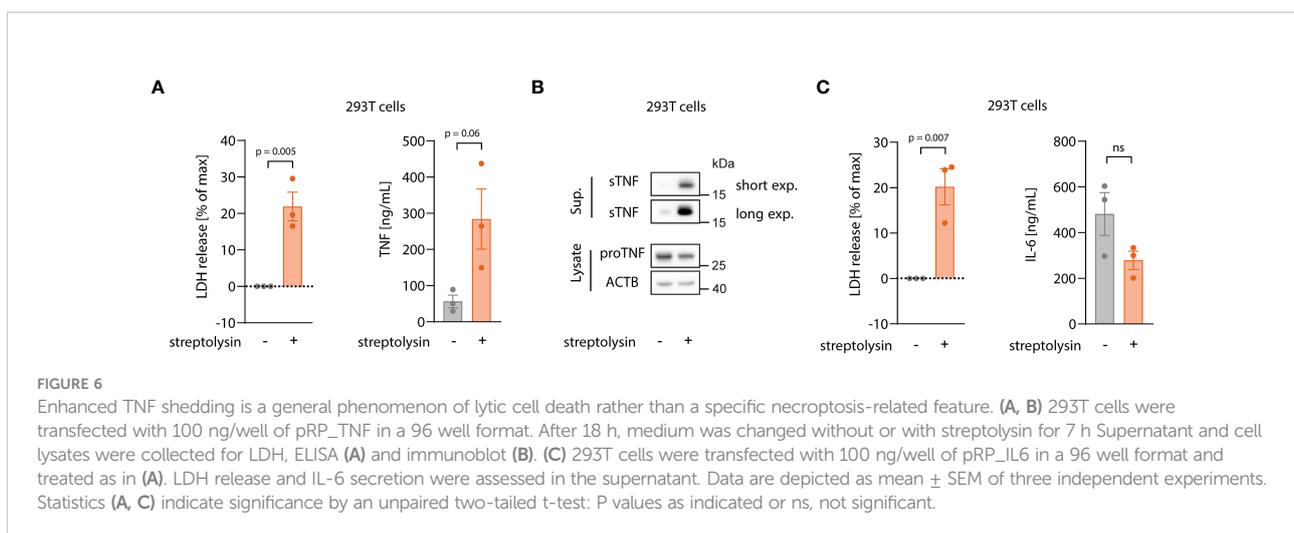## Necroptosis-driven TNF release in primary cells

Thus far our experiments had relied on cell lines to study the relevance and mechanism of necroptosis-induced TNF shedding. To explore whether these events also play a role in primary cells undergoing necroptosis, we turned to primary, human monocyte-derived macrophages (hMDM) as a model. Treating these cells with LPS and the pan-caspase inhibitor zVAD, resulted in a lytic cell death in approximately 25% of the cell population within an 8-hour timeframe (Figure 7A, left panel). Treatment with the specific RIPK3 inhibitor GSK'872 blocked this cell lysis, indicating that cells died by necroptosis. Analyzing TNF secretion revealed that necroptosis induction doubled the amount of released TNF, while it decreased IL-6 production by half (Figure 7A, middle and right panel). To employ a system that does not require LPS stimulation to induce necroptosis, we used murine macrophages derived from hematopoietic stem cells (HSCs). As such, we transduced HSCs with a murine RIPK3 construct that can be dimerized to induce necroptosis upon the addition of the small molecule drug AP20187 (Figure 7B) (46). After differentiation of these HSCs, these cells displayed a typical macrophage-like morphology and about 30% of them expressed the RIPK3 dimerizing construct, as judged by EGFP expression (Figures S5A, B). Indeed, RIPK3 dimerization by treatment with AP20187 induced lytic cell death specifically in transduced cells. Moreover, this synthetic
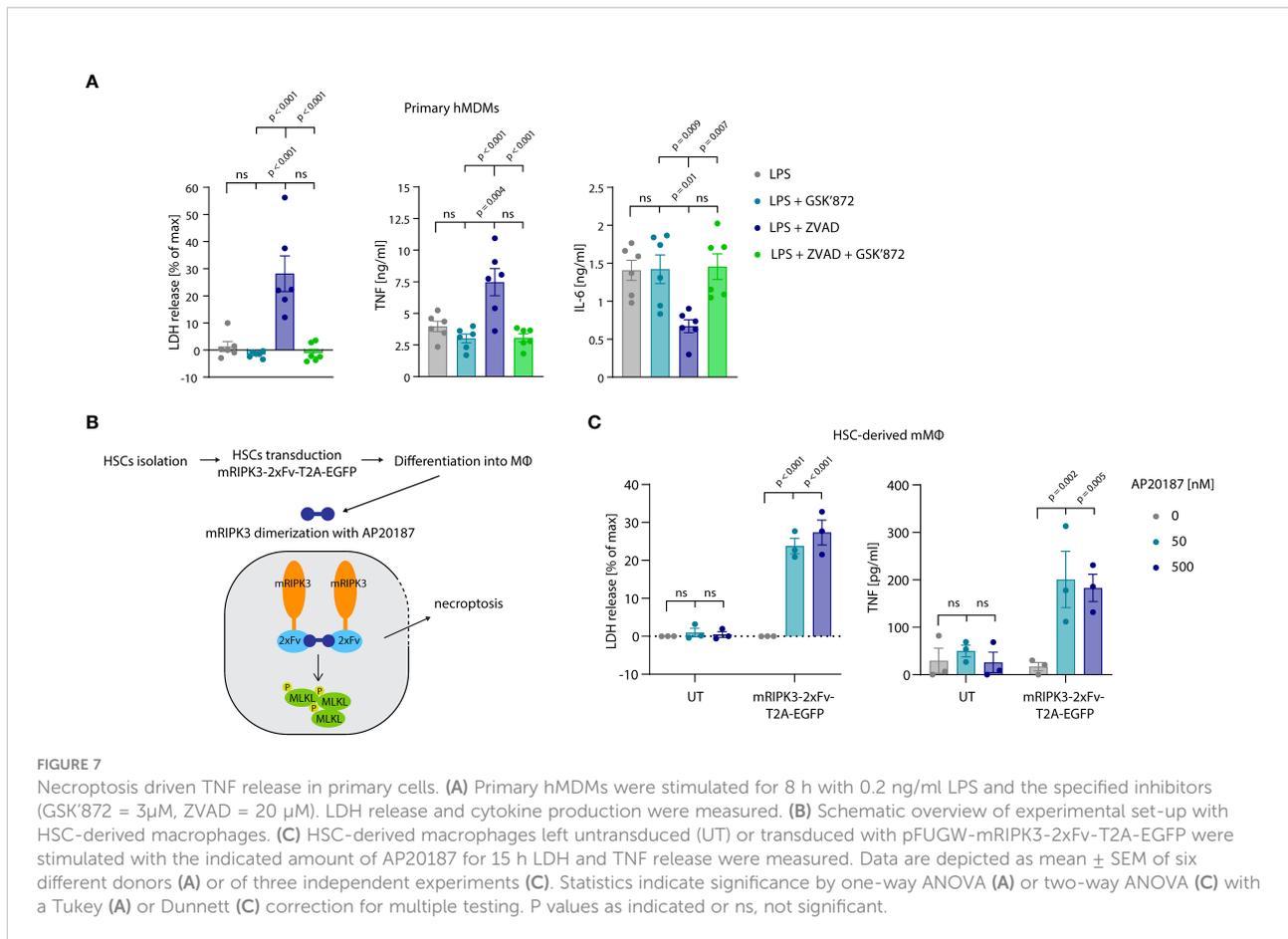
necroptosis-induction resulted in TNF release of these macrophages in the supernatant (Figure 7C). In summary, these results suggested that primary cells undergoing necroptosis also display enhanced TNF secretion.

Discussion

Necroptosis has emerged as a highly inflammatory form of regulated necrotic cell death. Numerous studies, primarily in genetic mouse models, provided experimental evidence that necroptotic cell death induces inflammation *in vivo*, suggesting that necroptosis may also be involved in the pathogenesis of human inflammatory diseases. However, the mechanisms by which necroptotic cells trigger inflammatory responses in the tissue microenvironment remain poorly understood. While genetic *in vivo* models are well-suited to characterize the impact of individual candidate factors on the organismic and tissue level, it is laborious and technically difficult to establish mechanistic relationships between putative DAMP or alarmin molecules being released and their pro-inflammatory activity. A major difficulty for such ventures is the dissection of the cellular source and target for putative inflammatory signals in a biologically redundant and dynamic system. Moreover, it is inherently challenging to discover and characterize novel DAMPs and/or alarmin(s) in the *in vivo* context.

We therefore developed a reductionist *in vitro* setting, in which necroptosis-driven inflammatory pathways can be addressed by genetically manipulating donor and recipient cells. To do so, we employed a myeloid cell system, in which we could recapitulate the phenomenon of necroptosis-driven pro-inflammatory gene expression. In this setup, we observed a strong, necroptosis-dependent NF-κB response in recipient cells when either co-cultured with necroptosing cells or exposed to their supernatant. The pro-inflammatory activity of this

FIGURE 6

Enhanced TNF shedding is a general phenomenon of lytic cell death rather than a specific necroptosis-related feature. **(A, B)** 293T cells were transfected with 100 ng/well of pRP_TNF in a 96 well format. After 18 h, medium was changed without or with streptolysin for 7 h Supernatant and cell lysates were collected for LDH, ELISA **(A)** and immunoblot **(B)**. **(C)** 293T cells were transfected with 100 ng/well of pRP_IL6 in a 96 well format and treated as in **(A)**. LDH release and IL-6 secretion were assessed in the supernatant. Data are depicted as mean $\pm$ SEM of three independent experiments. Statistics **(A, C)** indicate significance by an unpaired two-tailed t-test: P values as indicated or ns, not significant.

FIGURE 7

Necroptosis driven TNF release in primary cells. **(A)** Primary hMDMs were stimulated for 8 h with 0.2 ng/ml LPS and the specified inhibitors (GSK'872 = 3µM, ZVAD = 20 µM). LDH release and cytokine production were measured. **(B)** Schematic overview of experimental set-up with HSC-derived macrophages. **(C)** HSC-derived macrophages left untransduced (UT) or transduced with pFUGW-mRIPK3-2xFv-T2A-EGFP were stimulated with the indicated amount of AP20187 for 15 h LDH and TNF release were measured. Data are depicted as mean $\pm$ SEM of six different donors **(A)** or of three independent experiments **(C)**. Statistics indicate significance by one-way ANOVA **(A)** or two-way ANOVA **(C)** with a Tukey **(A)** or Dunnett **(C)** correction for multiple testing. P values as indicated or ns, not significant.

supernatant could be further narrowed down to be a heat-sensitive factor that could be resolved by size exclusion chromatography. Systematic perturbation of sensing and signal transduction cascades in recipient cells provided the surprising notion that this pro-inflammatory activity could be largely ascribed to TNF. Indeed, deleting *TNF* in necroptotic cells or *TNFRSF1A* in recipient cells, led to a complete loss of IL-6 release, indicating that NF-κB activation in this system is fully dependent on the TNF-TNFR1 axis (Figure S6).

TLR4-activated *CASP8*$^{-/-}$ cells released far more TNF into the supernatant compared to their *CASP8*$^{-/-}$ x *MLKL*$^{-/-}$ counterparts, which could be ascribed to two mechanisms: on the one hand, cells undergoing necroptosis produced more pro-TNF at the protein level than necroptosis-resistant cells. Of note, the expression of other pro-inflammatory mediators was not increased under these conditions. Moreover, heightened pro-TNF levels were not due to increased pro-TNF expression at the mRNA level, indicating that post-transcriptional mechanisms are operational. These results therefore implied that necroptosis blocks an inhibitory mechanism that regulates TNF expression at the post-transcriptional level through its 3' UTR. In line with this notion, LPS-stimulated cells undergoing necroptosis, yet lacking the TNF 3´UTR, showed similar amounts of pro-TNF

expression as non-necroptosing cells, while TNF levels were strongly increased under these conditions. Mechanistically, it is conceivable that certain TNF 3' UTR trans-activating factors are selectively depleted in the course of necroptosis or that certain post-translational modifications block their activity. Previous work has established that cells undergoing necroptosis indeed do not shut down protein synthesis (47) and that pro-inflammatory cytokine expression even proceeds in cells irreversibly committed to death upon the loss of cell membrane integrity (48). However, since pro-TNF requires further post-translational maturation at the plasma membrane, heightened pro-TNF expression levels by themselves would not be able to explain how necroptosis boosts the release of mature TNF. Indeed, we also observed that necroptosis strongly enhanced TNF shedding. We focused on this latter phenomenon in the following, since this mechanism likely constitutes the rate-limiting step in mature TNF secretion under these conditions. Moreover, this mechanism is universally applicable to cells undergoing necroptosis in the absence of a strong TNF-triggering stimulus such as the PAMP LPS used here. Indeed, cells heterologously expressing TNF displayed a strong increase in TNF maturation upon necroptosis induction, which was dependent on ADAM10/17. This is in line with previous

studies that found that ADAM proteases are activated upon necroptosis (49, 50). By studying TNF shedding in live cell imaging experiments, we observed that cells undergoing necroptosis displayed a far higher signal for TNF shedding at the single-cell level and that necroptosis-associated TNF maturation occurred with faster kinetics compared to control cells. In addition, we found that living cells shed TNF before MLKL-dependent membrane rupture. In particular, TNF shedding preceded PI uptake by almost one hour and it also occurred prior to Annexin V positivity. While these results would preclude phosphatidylserine (PS) exposure as the decisive factor for ADAM17 activation as previously reported (51), it cannot be excluded that PS exposure below the detection limit of our assay is of relevance.

To determine whether ADAM-dependent TNF release is a specific feature of necroptosis or applies generally to lytic types of cell death, we induced a necroptosis-independent type of lytic cell death using a bacterial pore-forming toxin. As such, we extracellularly added SLO, which assembles into large heterogeneous pores of 30–50 nm in diameter (52). Surpassing a critical concentration that cannot be repaired, SLO pores have been shown to trigger plasma membrane rupture and thus complete cell lysis. Indeed, employing SLO to induce plasma membrane permeability, we observed massive TNF shedding in cells heterologously expressing TNF. Therefore, we can exclude that a necroptosis-specific signaling molecule or unique aspect of its lytic cell death is required to trigger ADAM activity. We rather speculate that changes of the biophysical properties of the plasma membrane constitute the common denominator of ADAM activation, yet the exact mechanism of this phenomenon requires future studies. In this context, the involvement of protein kinase C (PKC) isoforms is likely, as this enzyme family is involved in the activation of ADAM17 (53). In addition, it should be noted that enhanced TNF secretion has not been reported in the context of inflammasome activation, which triggers pyroptosis, another form of lytic cell death (e.g (30)). We attribute this fact to differences in kinetics of necroptosis and pyroptosis. In fact, pyroptosis proceeds much faster compared to necroptosis, significantly reducing the time available for pro-TNF production and shedding into its mature form.

Importantly, our findings could be reproduced in primary cell systems, also when using different necroptosis-inducing strategies. Both human monocyte-derived macrophages, as well as murine HSC-derived macrophages displayed an increase in TNF release upon necroptosis induction. Given the constitutive expression of TNF in the latter system, we could also make use of a genetic model that did not require a pro-inflammatory signal to induce TNF expression. Addressing the role of TNF in necroptosis-driven inflammation *in vivo* is difficult since TNF also acts upstream of necroptosis induction. Indeed, several genetic models of necroptosis have shown a beneficial role for TNFR1 or TNF ablation in ameliorating necroptosis associated inflammation (54–59), and thus far this has been attributed to the TNF-TNFR1 axis to

induce necroptosis. However, it is reasonable to speculate that ablation of TNFR1 also affects the inflammatory response in these models by preventing activation of bystander cells through necroptosis-associated release of TNF. Such a scenario would position TNF in a vicious cycle, in which TNF-triggered necroptosis can result in the release of TNF itself.

Although TNF plays an almost non-redundant role as a pro-inflammatory mediator in our system, additional DAMPs or alarmins downstream of necroptosis cannot be excluded. Indeed, being limited to the reductionist *in vitro* culture conditions tested here, our system cannot account for the complexity of an *in vivo* setting, in which multiple different cell types interact in a dynamic crosstalk. Moreover, by using IL-6 as a proxy for the inflammatory response, it should also be noted that our model was only designed to identify NF-κB-activating factors. Finally, by using LPS as a necroptosis-inducing signal, we had to delete TLR4 in recipient cells, which excludes numerous DAMPs that have been described to engage this PRR.

In summary, we established necroptotic cells as a key source of TNF secretion. Conceptually - in light of the here-uncovered mode of action - TNF qualifies as an alarmin molecule that is released upon cell damage. The success of anti-TNF therapies in diseases characterized by chronic inflammation may be partially explained by uncontrolled necroptosis enhancing TNF production. Importantly, the identification of TNF as a necroptosis-associated alarmin may provide the rationale for the future application of anti-TNF agents to treat pathologies with an established role of necroptosis as a driver of inflammation.

Materials and methods

Cell culture

BLaER1 (60) and THP-1 (DSMZ, ACC 16) cells were cultured in RPMI medium 1640, supplemented with 10% (v/v) FCS, 1% sodium pyruvate (v/v), 100 U/ml Penicillin-Streptomycin (all Gibco). BLaER1 cells were trans-differentiated for 5-6 day in medium containing 10 ng/ml IL-3, 10 ng/ml M-CSF (MPI of Biochemistry, Munich) and 100 nM β-estradiol (Sigma-Aldrich) at a concentration of 7 x 10^4 cells/well in 96 well plates. Unless otherwise stated, $CASP4^{-/-}$ BLaER1 cells were used as genetic background to generate subsequent knock-out clones analyzed in this work. 293T cells (DSMZ, ACC 635) were cultured in DMEM supplemented as above.

Chemicals, peptides and recombinant proteins

The following reagents were purchased from commercial suppliers: Alexa Fluor® 647 Annexin V (Biolegend, Cat#640911),

B/B homodimerizer (Takara Bio, Cat#635058), b-estradiol (Sigma-Aldrich, Cat#E8875-250MG), CLI-095 (*In vivo*Gen, Cat# tlrl-cli95), Collagen R solution 0.2% (Serva, Cat#47254.02), DNAse I (Thermo Fisher Scientific, Cat#EN0525), Doxycycline hyclate (Sigma-Aldrich, Cat#D9891), eBioscience™ Propidium Iodide Staining Solution (Thermo Fisher Scientific, Cat# 00-6990-50), GeneJuice®Transfection Reagent (Merck Chemicals GmbH, Cat#70967), GeneRuler 1 kb DNA Ladder (Thermo Scientific, Cat# SM0311), GSK'872 (Aobious, Cat#AOB4887), Hepes 1M (Sigma-Aldrich, Cat#H0887-100ML), HT-DNA (Sigma-Aldrich, Cat#D6898), Lipofectamine 2000 (Life Technologies, Cat#11668019), LPS-EB Ultrapure (*In vivo*Gen, Cat#tlrl-3pelps), MCC950 (Sigma-Aldrich, Cat#5381200001), MEM Non-Essential Amino Acids Solution (100x) (Thermo Fisher Scientific, Cat#11140050), PageRuler™ Prestained Protein Ladder (Thermo Fisher Scientific, Cat#26617), Penicillin-Streptomycin (Life Technologies, Cat#15140122), Phorbol 12-myristate 13-acetate (Enzo Life Sciences, Cat#BML-PE160-0005), R848 (*In vivo*Gen, Cat# tlrl-r848), Recombinant Human TNF (Peprotech, Cat#300-01A), RetroNectin® Recombinant Human Fibronectin Fragment (Takara Bio, Cat#T100A), Recombinant Murine Flt3-Ligand (Peprotech, Cat#250-31L), Recombinant Murine IL-3 (Peprotech, Cat#213-13), Recombinant Murine IL-6 (Peprotech, Cat#216-16), Recombinant Murine SCF (Peprotech, Cat#250-03), Recombinant Murine TPO (Peprotech, Cat#315-14), Retronectin (Takara Bio Cat#T100A), Sodium Pyruvate (Thermo Fisher Scientific, Cat#11360088), Streptolysin O (Sigma-Aldrich, Cat# S5265-25KU), Z-VAD-FMK (Peptanova, Cat#3188-v).

Antibodies

The following antibodies were purchased from commercial suppliers: Alexa-488-conjugated secondary antibody (Thermo Fisher Scientific, Cat# A-11001, RRID : AB_2534069 and Cat# A-11008, RRID : AB_143165), anti-b-actin (C4) HRP (Santa Cruz Biotechnology, Cat# sc-47778 HRP, RRID : AB_271418), anti-Caspase-8 (1C12) (Cell Signaling Technology, Cat# 9746, RRID : AB_2275120), anti-ADAM10, CT (Millipore, Cat# AB19026, RRID : AB_2242320), anti-ADAM17 (D22H4) (Cell Signaling Technology, Cat# 6978, RRID : AB_1082838), anti-IκBα (L35A5) (Cell Signaling Technology, Cat# 4814, RRID : AB_390781), anti-phospho-IkBa (14D4) (Cell Signaling Technology, Cat# 2859, RRID : AB_561111), anti-TNF (D5G9) (Cell Signaling Technology, Cat# 6945, RRID : AB_10859375), CaptureSelect™ Alexa488 anti-C-tag conjugate (Thermo Fisher Scientific, Cat#7213252100), MLKL polyclonal antibody (Thermo Fisher Scientific, Cat# PA5-34733, RRID : AB_2552085), phospho-NF-κB p65 (Ser536) (93H1) rabbit mAb (Cell Signaling Technology, Cat# 3033, RRID : AB_331284), recombinant anti-MLKL (phospho S358) antibody (Abcam, Cat# ab187091, RRID : AB_2619685).

Derivation of human monocyte-derived macrophages

PBMCs were obtained from healthy volunteers. Informed consent was obtained from all subjects according to the Declaration of Helsinki and approval by the responsible ethical committee (project number 19-238, Ethics committee of the medical faculty of the Ludwig Maximilian University Munich). Monocytes were isolated using the CD14 positive selection method of MACS technology (Miltenyi Biotec, Cat#130-050-201) according to manufacturer's protocol. Purified monocytes were plated in 96 well plates (0.1 x 10^6 cells/well) and differentiated into monocytes-derived macrophages (MDMs) for 7-8 days in RPMI medium 1640 supplemented with 10% (v/v) FCS, 1% (v/v) sodium pyruvate, 1% (v/v) non-essential amino acids (Gibco), 100 U/ml Penicillin-Streptomycin and 100 ng/ml M-CSF (Peprotech).

Plasmids

Cloning of genes of interest into pLI, pRP, pFUGW and pEF-BOS backbones was performed by conventional restriction enzyme cloning. hTNF, $MLKL^{1-154}$ and $MLKL^{1-201}$ were amplified from cDNA of BLaER1 cells. The codon-optimized sequence of hIL6 was ordered from IDT. pMDLg/pRRE was a gift from Didier Trono (Addgene plasmid #12251; http://n2t.net/addgene:12251; RRID : Addgene_12251), pRSV-Rev was a gift from Didier Trono (Addgene plasmid #12253; http://n2t.net/addgene:12253; RRID : Addgene_12253), pLIX_403 (herin referred to as pLI) was a gift from David Root (Addgene plasmid #41395; http://n2t.net/addgene:41395; RRID : Addgene_41395).

Cell stimulations

Unless otherwise indicated, $CASP8^{-/-}$, $CASP8^{-/-}$ x $MLKL^{-/-}$ and subsequently derived gene-deficient BLaER1 macrophages were stimulated with 2 ng/ml LPS from *E. coli* (*In vivo*gen) for 18 h. In case of supernatant transfer experiment, the supernatant was then collected, centrifuged at 600 g for 5 minutes and used undiluted to stimulate $TLR4^{-/-}$ recipient BLaER1 cells for 24 h. When recipient cells were not in a $TLR4^{-/-}$ background, the TLR4 inhibitor CLI095 was added to the collected supernatant at the final concentration of 1 μg/ml. For co-culture experiments, $CASP8^{-/-}$ or $CASP8^{-/-}$ x $MLKL^{-/-}$ BLaER1 macrophages were mixed 1:1 with $TLR4^{-/-}$ cells and stimulated for 18 h with 2 ng/ml of LPS. For heat shock experiments, the supernatant of donor cells was heated at 75°C for 10 minutes before stimulation of $TLR4^{-/-}$ BLaER1 macrophages. FCS was replaced to a final concentration of 10% after heat shock treatment. The NLRP3 inhibitor MCC950 was used at the final concentration of 5 μM.

Stimulation of BLaER1 macrophages with other immune ligands was performed as follows: hTNF (Peprotech) 100 ng/ml, R848 (*In vivo*gen) 1 μg/ml for 16 h. 200 ng/well of IVT4 or herring testes DNA (HT-DNA, Sigma-Aldrich) were complexed with Lipofectamine 2000 (Life technologies) according to manufacturer's protocol and cells were stimulated with the mix for 16 h. Primary MDMs were stimulated with 0.2 ng/ml LPS for 8 h. The Caspase-8 inhibitor Z-VAD-FMK (Peptanova) and the RIPK3 inhibitor GSK'872 (Aobious) were added to the cells together with LPS at the final concentration of 20 μM and 3 μM, respectively. For the size exclusion chromatography experiment, THP-1 cells previously transduced with pLI-MLKL[1-201] were differentiated with 100 ng/ml PMA (Sigma-Aldrich) for 24 h before stimulation. Differentiation medium was removed, and cells were washed in PBS before incubation in serum-free medium in presence or absence of doxycycline (1 μg/ml) for 16 h. Doxycycline was used to stimulate 293T cells at the final concentration of 1 μg/ml for 7 h on the day after transfection. In case an immunoblot had to be performed, 293T and BLaER1 cells were stimulated respectively in 1% FCS or 3% FCS containing medium. To induce necroptosis in HSCs-derived macrophages transduced with the dimerizing construct (mRIPK3-2xFv-T2A-EGFP), cells were stimulated with indicated concentrations of B/B homodimerizer (Takara Bio) for 15 h. Streptolysin O was used at the concentration of 8 μg/ml for 7 h to stimulate 293T cells.

Derivation of macrophages from HSC

Hematopoietic stem cells (HSCs) were obtained from 8-weeks old wild-type C57BL/6 mice. Bone marrow was flushed from femurs and tibias and HSCs were isolated by negative selection with the Direct Lineage Depletion Kit (Miltenyi Biotec, Cat#130-110-470) using MACS technology. Isolated HSCs were cultured in StemPro[TM]-34 SFM (1X) media (Gibco) supplemented with StemPro®-Nutrient Supplement, 100 U/ml penicillin-streptomycin and the following cytokines (all PeproTech): IL-3 (10 ng/ml), FLT3-L (10 ng/ml), SCF (100 ng/ml), TPO (20 ng/ml), IL-6 (20 ng/ml). The day after isolation, HSCs were transduced as described. 24 h later, HSCs were plated in 96 well plate at 0.7 x 10^{5}/well and differentiated into macrophages in fully supplemented DMEM with 100 ng/ml M-CSF for 5 days. Medium with fresh M-CSF was added on day 2 or 3 after plating. All mice were handled according to institutional guidelines approved by the animal welfare and use committee of the government of Upper Bavaria.

CRISPR/Cas9 mediated gene ablation

BLaER1 and 293T cells deficient for specific genes were generated *via* CRISPR/Cas9 mediated gene ablation as

previously described ([61](#)). Briefly, sgRNAs were designed to target early codons of selected genes. pLK0.1-gRNA-CMV-GFP and a Cas9 expression plasmid (pRZ-BFP-Cas9) were co-electroporated in BLaER1 cells using a Biorad GenePulser device or co-transfected in 293T cells in combination with GeneJuice transfection reagent (Merck). 24 h later, cells positive for respective fluorescent markers were sorted and subjected to limiting dilution cloning. After 3-4 weeks, monoclones were identified and subjected to deep sequencing (Illumina Miseq platform). Clones bearing frameshift mutations were utilized for subsequent experiments. For the generation of TNF Δ 3′ UTR clones, 2 gRNAs targeting the very beginning and the very end of the 3′UTR of the TNF gene were cloned into pMini-U6-gRNA-CMV-BFP-T2A-Cas9 or pMini-U6-gRNA-CMV-mCherry-T2A-Cas9 and co-electroporated in BLaER1 parental cells. Double fluorescent cells were sorted and subjected to limiting dilution cloning. Clones lacking the 3′ UTR were selected by PCR on the target region using the following primers: fwd 5′ CCTGGTATGAGCCCATCTATCTG, rev 5′ TTCTTTTCTAAGCAAACTTTATTTCTCGCC (long product = WT, short product = Δ 3′UTR)

gRNA target sequences

The following genomic regions were targeted to generate knockout cell lines (PAM sequence is depicted in bold letters): ADAM17 GAGCAGAACATGATCCGGA**TGG**, ADAM10 TTTC AACCTACGAATGAAG**AGG**, LTA ACGTTCAGGTGGTGTC ATG**GGG**, TNF TGCAGCAGGCAGAAGAGCG**TGG**, MLKL GAGCTCTCGCTGTTACTTC**AGG**, TNFRS1A GCAGTCCGTA TCCTGCCCC**GGG**, TICAM1 (TRIF) GGCCCGCTTGTACC ACCTGC**TGG**, MAVS ACTTCATTGCGGCACTGAG**GGG**, STING1 GCGGGCCGACCGCATTTGGG**AGG**, MYD88 CTGC AGGAGGTCCCGGCGC**GGG**, CASP4 CTCATCCGAATA TGGAGGC**TGG**, IL6 TGTGGGGCGGCTACATCTT**TGG**, TLR4 GATAAAGTTCATAGGGTTC**AGG**, CASP8 GCTCAG GAACTTGAGGG**AGG,** TNF UTR (1) AGGGGGTAATAAA GGGATTG**GGG,** TNF UTR (2) TTACAGACACAACTCC CCTG**GGG.**

Virus production and cell transduction

For the generation of pseudotyped lentiviral particles, 293T cells were transfected by calcium phosphate co-precipitation with the lentiviral plasmid expressing the desired construct (in a pLI backbone) and the following packaging plasmids: pMDLg/pRRE, pRSV-REV and pCMV-VSVG. 8-14 h after transfection, medium was changed, and cells were incubated for 48-72 h before virus-containing supernatant was harvested and used to transduce target cells. Puromycin selection was applied for 3-4 days before further experimental use. To transduce HSCs with the dimerizing construct

(mRIPK3-2xFv-T2A-EGFP expressed in the lentiviral vector pFUGW), 0.5 x 10⁶ cells were plated in a 24-well pre-coated with retronectin (Takara Bio). Virus-containing medium was concentrated by ultracentrifugation and added to cells for 8 h. HSCs were then washed with PBS and transferred to a new 24-well with fresh culture medium. The percentage of transduced cells was evaluated by flow cytometry analysis of EGFP expression on the day of the experimental stimulation.

Immunoblotting

Cell pellets were lysed in cold RIPA buffer containing a cocktail of protease inhibitors (Roche, Cat# 11697498001). Quantification of proteins was conducted *via* the Pierce BCA Protein Assay Kit (Thermo Fisher Scientific, Cat#23227). Cell lysates and cell supernatants were denatured in Laemmli Buffer for 10 minutes at 95°C, followed by separation by denaturing SDS-PAGE. Equal amounts of proteins from lysates (15-20 µg) or equal volumes of supernatant were loaded in each lane. In the case of BLaER1 supernatant, proteins were precipitated with methanol/chloroform before denaturation in Laemmli buffer. Proteins were blotted onto a 0.2 µm nitrocellulose membrane, blocked in 5% milk and incubated with indicated primary antibody overnight at 4°C. The day after, membranes were washed and incubated in respective HRP-coupled secondary antibodies for 1 h at room temperature. Upon need, membranes were re-probed with multiple antibodies. Chemiluminescent signal was detected *via* a CCD camera (Fusion Fx, Vilber).

Transient transfection of 293T cells

293T cells were transfected with plasmid DNA complexed with GeneJuice following provider's instructions. For experiments where both immunoblotting and ELISA had to be performed, 0.65 x 10⁶ cells of indicated genotypes were plated in each well of a 6 well plate and transfected the day after, unless otherwise indicated. Co-transfection with 2 plasmids was performed by using 1.5 µg of each plasmid/well. Cells were used for the experiment on the day after transfection. When only ELISA analysis had to be performed, 2 x 10⁴ cells/well were plated in 96-well format and transfected the day after with 200 ng/well of the needed plasmids (100 ng/plasmid in case of co-transfection with 2 plasmids or in case of transfection followed by streptolysin O stimulation). For live cell imaging experiments, 1.7 x 10⁴ 293T cells of the indicated genotypes were plated in collagen R (Serva) coated Ibidi µ-Plate 96 well black (Ibidi) using FluoroBrite DMEM medium (Life Technologies) supplemented as described, with the addition of 10 mM Hepes (Sigma-Aldrich). The day after, cells were transfected with a total of

100 ng DNA/well (50 ng of pLI-C-tag-TNF linker mCherry or pLI-C-tag-TNF + 50 ng pEF-BOS-nBFP, the latter for the expression of a nuclear BFP). 24 h after transfection, cells were stimulated with doxycycline as described.

Live cell imaging

Imaging was performed starting 4 h after doxycycline treatment to induce the expression of MLKL$^{1-201}$ and/or C-tag TNF/C-tag TNF mCherry. Before imaging, the CaptureSelect™ Alexa Fluor™ 488 anti-C-tag conjugate (Thermo Fisher Scientific) was added to the cell supernatant at a final dilution of 1:480. When necessary, propidium iodide (eBioscience) was added to a final dilution of 1:250 and Annexin V Alexa Fluor™ 647 (Biolegend) was used at 1:125 dilution. Imaging was performed over a period of time of 4h 30 on a Leica DMi8 inverted microscope equipped with a HC PL APO 63x/1.20 W CORR CS2 objective, with a picture taken every 6 minutes. For image analysis, we used *FIJI* (https://imagej.net/) to select regions of interests in individual cells (their motilities were negligible over the observation time) and extract the fluorescence intensity trajectories for the individual fluorescent channels. Different fields of view of at least 3 independent experiments were utilized for the analysis. The mean fluorescence intensities were then plotted as a function of time for single cells and analyzed using *OriginPro2021* (OriginLab). In the case of induction of MLKL$^{1-201}$, an inflection point was visible in the fluorescence intensity trajectories corresponding to the Alexa488 channel (green lines in Figure 5B). We computed the maximal slopes at the inflection point time as a simple measurement of expression kinetics. In the other cases (WT control and *ADAM10$^{-/-}$* x *ADAM17$^{-/-}$* MLKL$^{1-201}$ cells), we calculated an average slope by performing a linear regression of the whole fluorescence intensity trajectories.

Size exclusion chromatography

THP1 cells were stimulated as described above in serum-free medium. Supernatant from doxycycline-induced or uninduced cells (40ml per condition) was collected and concentrated to 500 µL using Amicon Ultra-15 filters with 10 kDa cutoff (Merck Millipore). The concentrated samples were loaded on a Superose 6 10/300GL column (GE Healthcare) and an isocratic run (1.2 column volume) was conducted on an ÄKTA Basic instrument with a flowrate of 0.3 ml/min. Degassed and filtered PBS was used as running buffer. 500 µL fractions were collected and utilized for 14 h stimulation of *TLR4$^{-/-}$* BLaER1 recipient cells. Upon stimulation, fractions were diluted 1:1 with fully supplemented RPMI medium, adjusting the FCS content to 10% v/v.

RNA sequencing

Differentiated BLaER1 cells were left untreated or LPS stimulated for 2 h. Next, 3×10^6 cells were lysed in 1ml Trizol and library preparation performed as described elsewhere (62). The libraries were sequenced on an Illumina HiSeq1500 device. Reads were aligned to the human reference genome GRCh38 using STAR v.2.5.1 (63) and counted using the GenomicAlignments R package (64). Post mapping analysis was conducted in R (65). Normalization and scaling were performed using DESeq2's (66). GGplot2 (67) was used to visualize results.

RT-qPCR

RT-qPCR analysis of LPS stimulated BLaER1 cells of indicated genotypes was performed as follows. RNA from BLaER1 cells was purified *via* the Total RNA purification mini spin kit (Genaxxon, Cat#S5304.0250) and DNA digestion was performed with DNAse I (Thermo Fisher Scientific) incubation for 30 minutes. 700 ng of RNA was used for cDNA synthesis by RevertAid Reverse transcriptase (Thermo Fisher Scientific, Cat#EP0442) with oligo dT primers. qPCR reaction was performed with the PowerUp^{TM} SYBR^{TM} Green Master Mix (Thermo Fisher Scientific) in presence of primers specific for genes of interest: TNF_fwd: CAGGGACCTC TCTCTAATCAG, TNF_rev: TTGAGGGTTTGCTACAACATGG, TBP1_fwd: TATAATCCCAAGCGGTTTGC, TBP1_rev: CTGTTC TTCACTCTTGGCTCCT GUSB_fwd: CGCCCTGCCTATCTG TATTCATTGGAGGTG, GUSB_rev: GATGAGGAA CTGGCTCTTGGTGACAGCC. The average of GUSB and TBP1 housekeeping genes was used to calculate ΔCt, followed by calculation of the ΔΔCt using the untreated sample of each clone as control.

ELISA

hIL-6 (BD Biosciences, Cat#555220), hTNF (BD Biosciences, Cat#555212), hIL-8 ELISA (BD Biosciences, Cat#555244), hIL-1β ELISA (BD Biosciences, Cat#557953), hIP-10 (BD Biosciences, Cat#550926), mmTNF (BD Biosciences, Cat#558534) and hIL-6Rα ELISA (R&D Systems, Cat#DY227) were performed according to provider's protocol.

LDH

Pierce LDH Cytotoxicity Assay Kit (Thermo Fisher Scientific, Cat#C20301) was performed according to manufacturer's instructions. Relative LDH release was calculated as LDH release [%] = 100 * (measurement – unstimulated control)/(lysis control – unstimulated control). Because of the use of this equation, negative data can be obtained when LDH release is lower in a tested sample compared to the untreated control.

Quantification and statistical analysis

Statistical significance was determined as explained in the figure legends with the respective *post hoc* corrections for multiple testing, if relevant. If multiple comparisons are depicted with one comparison bar, the major tick of the comparison bar indicates the reference data to which the statements regarding the level of significance are made. Statistical analysis was performed with GraphPad Prism 8.

Data availability statement

The datasets presented in this study can be found in online repositories. The names of the repository/repositories and accession number(s) can be found below: https://www.ncbi. nlm.nih.gov/bioproject/PRJNA716479.

Ethics statement

Informed consent was obtained from all subjects according to the Declaration of Helsinki and approval by the responsible ethical committee (project number 19-238, Ethics committee of the medical faculty of the Ludwig Maximilian University Munich). The patients/participants provided their written informed consent to participate in this study. All mice were handled according to institutional guidelines approved by the animal welfare and use committee of the government of Upper Bavaria.

Author contributions

Conceptualization, FP, MG and VH. Formal analysis, GK and CJ. Investigation, FP, DN. Resources, MG. Writing, FP and VH with input from all authors. Funding acquisition, VH. Supervision, VH. All authors contributed to the article and approved the submitted version.

Funding

Acknowledgments

Niklas Schmacke (Gene Center, LMU) for deep sequencing, Joshua Kie from the BioSysM FACS Core Facility (Gene Center, LMU) for cell sorting as well as BioSysM Automation Unit.

Conflict of interest

The authors declare that the research was conducted in the absence of any commercial or financial relationships that could be construed as a potential conflict of interest.

Publisher's note

All claims expressed in this article are solely those of the authors and do not necessarily represent those of their affiliated organizations, or those of the publisher, the editors and the reviewers. Any product that may be evaluated in this article, or claim that may be made by its manufacturer, is not guaranteed or endorsed by the publisher.

Supplementary material

The Supplementary Material for this article can be found online at: https://www.frontiersin.org/articles/10.3389/fimmu.2022.1074440/full#supplementary-material

SUPPLEMENTARY VIDEO 1–3
Necroptosis induces TNF shedding in a switch-like fashion. 293T MLKL[1-201] (video 1), $ADAM10^{-/-}$ x $ADAM17^{-/-}$ MLKL[1-201] 293T (video 2) and 293T WT (video 3) were transfected with pLI-C-tag-TNF linker mCherry and pEF-BOS-nBFP, stimulated with 1 μg/ml doxycycline and imaged over time (1 image every 6 minutes). Overlay of brightfield, mCherry (TNF) and C-tag TNF is shown.

References

1. Chan FK, Luz NF, Moriwaki K. Programmed necrosis in the cross talk of cell death and inflammation. *Annu Rev Immunol* (2015) 33:79–106. doi: 10.1146/annurev-immunol-032414-112248

2. Cho YS, Challa S, Moquin D, Genga R, Ray TD, Guildford M, et al. Phosphorylation-driven assembly of the Rip1-Rip3 complex regulates programmed necrosis and virus-induced inflammation. *Cell* (2009) 137(6):1112–23. doi: 10.1016/j.cell.2009.05.037

3. Li J, McQuade T, Siemer AB, Napetschnig J, Moriwaki K, Hsiao Y-S, et al. The Rip1/Rip3 necrosome forms a functional amyloid signaling complex required for programmed necrosis. *Cell* (2012) 150(2):339–50. doi: 10.1016/j.cell.2012.06.019

4. Sun L, Wang H, Wang Z, He S, Chen S, Liao D, et al. Mixed lineage kinase domain-like protein mediates necrosis signaling downstream of Rip3 kinase. *Cell* (2012) 148(1-2):213–27. doi: 10.1016/j.cell.2011.11.031

5. Zhao J, Jitkaew S, Cai Z, Choksi S, Li Q, Luo J, et al. Mixed lineage kinase domain-like is a key receptor interacting protein 3 downstream component of tnf-induced necrosis. *Proc Natl Acad Sci* (2012) 109(14):5322. doi: 10.1073/pnas.1200012109

6. Murphy JM. The killer pseudokinase mixed lineage kinase domain-like protein (Mlkl). *Cold Spring Harbor Perspect Biol* (2020) 12(8). doi: 10.1101/cshperspect.a036376

7. He S, Liang Y, Shao F, Wang X. Toll-like receptors activate programmed necrosis in macrophages through a receptor-interacting kinase-3-Mediated pathway. *Proc Natl Acad Sci U.S.A.* (2011) 108(50):20054–9. doi: 10.1073/pnas.1116302108

8. Kaiser WJ, Sridharan H, Huang C, Mandal P, Upton JW, Gough PJ, et al. Toll-like receptor 3-mediated necrosis *Via* trif, Rip3, and mlkl. *J Biol Chem* (2013) 288(43):31268–79. doi: 10.1074/jbc.M113.462341

9. Rebsamen M, Heinz LX, Meylan E, Michallet M-C, Schroder K, Hofmann K, et al. Dai/Zbp1 recruits Rip1 and Rip3 through rip homotypic interaction motifs to activate nf-Kb. *EMBO Rep* (2009) 10(8):916–22. doi: 10.1038/embor.2009.109

10. Upton JW, Kaiser WJ, Mocarski ES. Dai/Zbp1/Dlm-1 complexes with Rip3 to mediate virus-induced programmed necrosis that is targeted by murine cytomegalovirus vira. *Cell Host Microbe* (2012) 11(3):290–7. doi: 10.1016/j.chom.2012.01.016

11. Sun X, Yin J, Starovasnik MA, Fairbrother WJ, Dixit VM. Identification of a novel homotypic interaction motif required for the phosphorylation of receptor-interacting protein (Rip) by Rip3*. *J Biol Chem* (2002) 277(11):9505–11. doi: 10.1074/jbc.M109488200

12. He S, Wang X. Rip kinases as modulators of inflammation and immunity. *Nat Immunol* (2018) 19(9):912–22. doi: 10.1038/s41590-018-0188-x

13. Gaidt MM, Ebert TS, Chauhan D, Schmidt T, Schmid-Burgk JL, Rapino F, et al. Human monocytes engage an alternative inflammasome pathway. *Immunity* (2016) 44(4):833–46. doi: 10.1016/j.immuni.2016.01.012

14. Lin Y, Devin A, Rodriguez Y, Liu Z-g. Cleavage of the death domain kinase rip by caspase-8 prompts tnf-induced apoptosis. *Genes Dev* (1999) 13(19):2514–26. doi: 10.1101/gad.13.19.2514

15. Feng S, Yang Y, Mei Y, Ma L, Zhu DE, Hoti N, et al. Cleavage of Rip3 inactivates its caspase-independent apoptosis pathway by removal of kinase domain. *Cell Signalling* (2007) 19(10):2056–67. doi: 10.1016/j.cellsig.2007.05.016

16. Mocarski ES, Upton JW, Kaiser WJ. Viral infection and the evolution of caspase 8-regulated apoptotic and necrotic death pathways. *Nat Rev Immunol* (2012) 12(2):79–88. doi: 10.1038/nri3131

17. Upton JW, Kaiser WJ, Mocarski ES. Virus inhibition of Rip3-dependent necrosis. *Cell Host Microbe* (2010) 7(4):302–13. doi: 10.1016/j.chom.2010.03.006

18. Petrie EJ, Sandow JJ, Lehmann WIL, Liang LY, Coursier D, Young SN, et al. Viral mlkl homologs subvert necroptotic cell death by sequestering cellular Ripk3. *Cell Rep* (2019) 28(13):3309–19.e5. doi: 10.1016/j.celrep.2019.08.055

19. Orzalli MH, Kagan JC. Apoptosis and necroptosis as host defense strategies to prevent viral infection. *Trends Cell Biol* (2017) 27(11):800–9. doi: 10.1016/j.tcb.2017.05.007

20. Pasparakis M, Vandenabeele P. Necroptosis and its role in inflammation. *Nature* (2015) 517(7534):311–20. doi: 10.1038/nature14191

21. Kaczmarek A, Vandenabeele P, Krysko DV. Necroptosis: The release of damage-associated molecular patterns and its physiological relevance. *Immunity* (2013) 38(2):209–23. doi: 10.1016/j.immuni.2013.02.003

22. Gunther C, Martini E, Wittkopf N, Amann K, Weigmann B, Neumann H, et al. Caspase-8 regulates tnf-Alpha-Induced epithelial necroptosis and terminal ileitis. *Nature* (2011) 477(7364):335–9. doi: 10.1038/nature10400

23. Lehle AS, Farin HF, Marquardt B, Michels BE, Magg T, Li Y, et al. Intestinal inflammation and dysregulated immunity in patients with inherited caspase-8 deficiency. *Gastroenterology* (2019) 156(1):275–8. doi: 10.1053/j.gastro.2018.09.041

24. Zhao H, Jaffer T, Eguchi S, Wang Z, Linkermann A, Ma D. Role of necroptosis in the pathogenesis of solid organ injury. *Cell Death Dis* (2015) 6 (11):e1975. doi: 10.1038/cddis.2015.316

25. Alvarez-Diaz S, Preaudet A, Samson AL, Nguyen PM, Fung KY, Garnham AL, et al. Necroptosis is dispensable for the development of inflammation-associated or sporadic colon cancer in mice. *Cell Death Differ* (2020) 28(5):1466–1476. doi: 10.1038/s41418-020-00673-z

26. Bertheloot D, Latz E. Hmgb1, il-1alpha, il-33 and S100 proteins: Dual-function alarmins. *Cell Mol Immunol* (2017) 14(1):43–64. doi: 10.1038/cmi.2016.34

27. Orozco S, Oberst A. Ripk3 in cell death and inflammation: The good, the bad, and the ugly. *Immunol Rev* (2017) 277(1):102–12. doi: 10.1111/imr.12536

28. Vince JE, Wong WW, Gentle I, Lawlor KE, Allam R, O'Reilly L, et al. Inhibitor of apoptosis proteins limit Rip3 kinase-dependent interleukin-1 activation. *Immunity* (2012) 36(2):215–27. doi: 10.1016/j.immuni.2012.01.012

29. Kang TB, Yang SH, Toth B, Kovalenko A, Wallach D. Caspase-8 blocks kinase Ripk3-mediated activation of the Nlrp3 inflammasome. *Immunity* (2013) 38 (1):27–40. doi: 10.1016/j.immuni.2012.09.015

30. Coll RC, Robertson AA, Chae JJ, Higgins SC, Munoz-Planillo R, Inserra MC, et al. A small-molecule inhibitor of the Nlrp3 inflammasome for the treatment of inflammatory diseases. *Nat Med* (2015) 21(3):248–55. doi: 10.1038/nm.3806

31. Arnez KH, Kindlova M, Bokil NJ, Murphy JM, Sweet MJ, Guncar G. Analysis of the n-terminal region of human mlkl, as well as two distinct mlkl isoforms, reveals new insights into necroptotic cell death. *Biosci Rep* (2015) 36(1): e00291. doi: 10.1042/BSR20150246

32. Taylor GA, Carballo E, Lee DM, Lai WS, Thompson MJ, Patel DD, et al. A pathogenetic role for tnf alpha in the syndrome of cachexia, arthritis, and autoimmunity resulting from tristetraprolin (Ttp) deficiency. *Immunity* (1996) 4 (5):445–54. doi: 10.1016/s1074-7613(00)80411-2

33. Kontoyiannis D, Pasparakis M, Pizarro TT, Cominelli F, Kollias G. Impaired on/Off regulation of tnf biosynthesis in mice lacking tnf au-rich elements: Implications for joint and gut-associated immunopathologies. *Immunity* (1999) 10(3):387–98. doi: 10.1016/s1074-7613(00)80038-2

34. Stoecklin G, Lu M, Rattenbacher B, Moroni C. A constitutive decay element promotes tumor necrosis factor alpha mrna degradation *Via* an au-rich element-independent pathway. *Mol Cell Biol* (2003) 23(10):3506–15. doi: 10.1128/MCB.23.10.3506-3515.2003

35. Androulidaki A, Iliopoulos D, Arranz A, Doxaki C, Schworer S, Zacharioudaki V, et al. The kinase Akt1 controls macrophage response to lipopolysaccharide by regulating micrornas. *Immunity* (2009) 31(2):220–31. doi: 10.1016/j.immuni.2009.06.024

36. Leppek K, Schott J, Reitter S, Poetz F, Hammond MC, Stoecklin G. Roquin promotes constitutive mrna decay *Via* a conserved class of stem-loop recognition motifs. *Cell* (2013) 153(4):869–81. doi: 10.1016/j.cell.2013.04.016

37. Lunn CA, Fan X, Dalie B, Miller K, Zavodny PJ, Narula SK, et al. Purification of Adam 10 from bovine spleen as a tnfalpha convertase. *FEBS Lett* (1997) 400(3):333–5. doi: 10.1016/s0014-5793(96)01410-x

38. Rosendahl MS, Ko SC, Long DL, Brewer MT, Rosenzweig B, Hedl E, et al. Identification and characterization of a pro-tumor necrosis factor-A-Processing enzyme from the Adam family of zinc metalloproteases. *J Biol Chem* (1997) 272 (39):24588–93. doi: 10.1074/jbc.272.39.24588

39. Moss ML, Jin SLC, Milla ME, Burkhart W, Carter HL, Chen W-J, et al. Cloning of a disintegrin metalloproteinase that processes precursor tumour-necrosis factor-A. *Nature* (1997) 385(6618):733–6. doi: 10.1038/385733a0

40. Black RA, Rauch CT, Kozlosky CJ, Peschon JJ, Slack JL, Wolfson MF, et al. A metalloproteinase disintegrin that releases tumour-necrosis factor-alpha from cells. *Nature* (1997) 385(6618):729–33. doi: 10.1038/385729a0

41. Pinci F, Gaidt MM, Jung C, Kuut G, Jackson MA, Bauernfried S, et al. C-tag tnf: A reporter system to study tnf shedding. *J Biol Chem* (2020) 295(52):18065–75. doi: 10.1074/jbc.RA120.015248

42. Müllberg J, Schooltink H, Stoyan T, Günther M, Graeve L, Buse G, et al. The soluble interleukin-6 receptor is generated by shedding. *Eur J Immunol* (1993) 23 (2):473–80. doi: 10.1002/eji.1830230226

43. Zargarian S, Shlomovitz I, Erlich Z, Hourizadeh A, Ofir-Birin Y, Croker BA, et al. Phosphatidylserine externalization, "Necroptotic bodies" release, and phagocytosis during necroptosis. *PloS Biol* (2017) 15(6):e2002711. doi: 10.1371/journal.pbio.2002711

44. Bhakdi S, Tranum-Jensen J, Sziegoleit A. Mechanism of membrane damage by streptolysin-O. *Infect Immun* (1985) 47(1):52–60. doi: 10.1128/iai.47.1.52-60.1985

45. Los FC, Randis TM, Aroian RV, Ratner AJ. Role of pore-forming toxins in bacterial infectious diseases. *Microbiol Mol Biol Rev* (2013) 77(2):173–207. doi: 10.1128/MMBR.00052-12

46. Orozco S, Yatim N, Werner MR, Tran H, Gunja SY, Tait SW, et al. Ripk1 both positively and negatively regulates Ripk3 oligomerization and necroptosis. *Cell Death Differ* (2014) 21(10):1511–21. doi: 10.1038/cdd.2014.76

47. Saelens X, Festjens N, Parthoens E, Vanoverberghe I, Kalai M, van Kuppeveld F, et al. Protein synthesis persists during necrotic cell death. *J Cell Biol* (2005) 168(4):545–51. doi: 10.1083/jcb.200407162

48. Orozco SL, Daniels BP, Yatim N, Messmer MN, Quarato G, Chen-Harris H, et al. Ripk3 activation leads to cytokine synthesis that continues after loss of cell membrane integrity. *Cell Rep* (2019) 28(9):2275–87 e5. doi: 10.1016/j.celrep.2019.07.077

49. Cai Z, Zhang A, Choksi S, Li W, Li T, Zhang XM, et al. Activation of cell-surface proteases promotes necroptosis, inflammation and cell migration. *Cell Res* (2016) 26(8):886–900. doi: 10.1038/cr.2016.87

50. Tanzer MC, Frauenstein A, Stafford CA, Phulphagar K, Mann M, Meissner F. Quantitative and dynamic catalogs of proteins released during apoptotic and necroptotic cell death. *Cell Rep* (2020) 30(4):1260–70 e5. doi: 10.1016/j.celrep.2019.12.079

51. Sommer A, Kordowski F, Buch J, Maretzky T, Evers A, Andra J, et al. Phosphatidylserine exposure is required for Adam17 sheddase function. *Nat Commun* (2016) 7:11523. doi: 10.1038/ncomms11523

52. Brito C, Cabanes D, Sarmento Mesquita F, Sousa S. Mechanisms protecting host cells against bacterial pore-forming toxins. *Cell Mol Life Sci* (2019) 76 (7):1319–39. doi: 10.1007/s00018-018-2992-8

53. Kveiborg M, Instrell R, Rowlands C, Howell M, Parker PJ. Pkcalpha and pkcdelta regulate Adam17-mediated ectodomain shedding of heparin binding-egf through separate pathways. *PloS One* (2011) 6(2):e17168. doi: 10.1371/journal.pone.0017168

54. Pasparakis M, Courtois G, Hafner M, Schmidt-Supprian M, Nenci A, Toksoy A, et al. Tnf-mediated inflammatory skin disease in mice with epidermis-specific deletion of Ikk2. *Nature* (2002) 417(6891):861–6. doi: 10.1038/nature00820

55. Bonnet MC, Preukschat D, Welz PS, van Loo G, Ermolaeva MA, Bloch W, et al. The adaptor protein fadd protects epidermal keratinocytes from necroptosis *in vivo* and prevents skin inflammation. *Immunity* (2011) 35(4):572–82. doi: 10.1016/j.immuni.2011.08.014

56. Ofengeim D, Ito Y, Najafov A, Zhang Y, Shan B, DeWitt Judy P, et al. Activation of necroptosis in multiple sclerosis. *Cell Rep* (2015) 10(11):1836–49. doi: 10.1016/j.celrep.2015.02.051

57. Welz PS, Wullaert A, Vlantis K, Kondylis V, Fernandez-Majada V, Ermolaeva M, et al. Fadd prevents Rip3-mediated epithelial cell necrosis and chronic intestinal inflammation. *Nature* (2011) 477(7364):330–4. doi: 10.1038/nature10273

58. Dannappel M, Vlantis K, Kumari S, Polykratis A, Kim C, Wachsmuth L, et al. Ripk1 maintains epithelial homeostasis by inhibiting apoptosis and necroptosis. *Nature* (2014) 513(7516):90–4. doi: 10.1038/nature13608

59. Schwarzer R, Jiao H, Wachsmuth L, Tresch A, Pasparakis M. Fadd and caspase-8 regulate gut homeostasis and inflammation by controlling mlkl- and gsdmd-mediated death of intestinal epithelial cells. *Immunity* (2020) 52(6):978–93.e6. doi: 10.1016/j.immuni.2020.04.002

60. Rapino F, Robles EF, Richter-Larrea JA, Kallin EM, Martinez-Climent JA, Graf T. C/Ebpalpha induces highly efficient macrophage transdifferentiation of b lymphoma and leukemia cell lines and impairs their tumorigenicity. *Cell Rep* (2013) 3(4):1153–63. doi: 10.1016/j.celrep.2013.03.003

61. Schmid-Burgk JL, Schmidt T, Gaidt MM, Pelka K, Latz E, Ebert TS, et al. Outknocker: A web tool for rapid and simple genotyping of designer nuclease edited cell lines. *Genome Res* (2014) 24(10):1719–23. doi: 10.1101/gr.176701.114

62. Greulich W, Wagner M, Gaidt MM, Stafford C, Cheng Y, Linder A, et al. Tlr8 is a sensor of rnase T2 degradation products. *Cell* (2019) 179(6):1264–75.e13. doi: 10.1016/j.cell.2019.11.001

63. Dobin A, Davis CA, Schlesinger F, Drenkow J, Zaleski C, Jha S, et al. Star: Ultrafast universal rna-seq aligner. *Bioinf (Oxford England)* (2013) 29(1):15–21. doi: 10.1093/bioinformatics/bts635

64. Lawrence M, Huber W, Pagès H, Aboyoun P, Carlson M, Gentleman R, et al. Software for computing and annotating genomic ranges. *PloS Comput Biol* (2013) 9(8):e1003118. doi: 10.1371/journal.pcbi.1003118

65. Team RC. *R core team (2020). r: A language and environment for statistical computing*. Vienna, Austria: R Foundation for Statistical Computing (2020).

66. Love MI, Huber W, Anders S. Moderated estimation of fold change and dispersion for rna-seq data with Deseq2. *Genome Biol* (2014) 15(12):550. doi: 10.1186/s13059-014-0550-8

67. Ginestet C. Ggplot2: Elegant graphics for data analysis. *J R Stat Soc: Ser A (Statistics Society)* (2011) 174(1):245–6. doi: 10.1111/j.1467-985X.2010.00676_9.x